University of Calif. San Diego.

FINAL REPORT NAG5-610

81 P.

ANALYTIC (1+2)

During the two years that this grant was in effect, we completed a large number of the tasks that were proposed in the original three year effort. The remaining tasks are being accomplished on the contract at the University of Alabama in Huntsville. In particular, we designed and constructed PCM encoder capable of storing data on-board into the mass-memory in the encoder at up to 12 megabits per second (total memory of 8 megabytes). This telemetry system was programed for two successful flights. The first flight was launched in March 1983 from Pokerflat, Alaska. The second, the Greenland One Campaign, flew in December/January of 1985. The remaining flight, the Critical Velocity Effort, will be launched in May of 1986. All parts of the electronic system functioned perfectly during both previous flights and the detectors performed perfectly. However, in the first flight in Pokerflat, Alaska, an electron arm did not deploy for reasons as yet unknown. The ion arm deployed perfectly and good data was acquired.

The Greenland flights were spectacularly successful in that all elements of the detector system, along with co-investigator experiments, functioned perfectly. Efforts are now under way to get these results into the literature and AGU presentations in the Spring of 1986. In the data analysis area, we have pursued the data analysis of the Condor Critical Velocity Experiment which has resulted in several papers included in the appendix, as well as one PhD thesis. The Condor experiment stimulated a few independant, theoretical investigations, as well as our own continued analysis. We are hopeful that a recent model of these releases will help to determine perameters that we will use on the launch of the Crit I experiment during the Spring of the year. These results will also be presented in an invited talk at the COSPAR in July, 1986.

The electronic system we designed consists of a Main Processor which controls all elements of the encoder. The I/O periferals may be accessed either by the processor or under automated control via a DMA sequencer. The

DMA sequencer allows for the very fast burst capture that would not be possible with a regular processor. Thus, the encoder can be run in either of two modes--one being, without the DMA under total processor control. In this case, we are highly software intensive and require a large software effort to implement our storage. This is the system that was employed on both the Pokerflat and Greenland flights. The DMA system will be employed during the Crit I experiment and will allow for very fast burst capture, in this case, a rate of three megabits per second into one megabyte of memory.

The processor controls the acquisition of analog digital data through several subsystems. The first subsystem is the analog-to-digital convertor system which has two different possibilities. The first possibility is a slow acquisition system of some 40 kilosamples per second at 12 bits into 32 separate channels. The second is a fast system capable of up to 500,000 kilosamples per second at 12 bits divided into 16 channels.

Particle data is accumulated into 16 bit accumulators based on the Intel 82C54 counter timer chip. These accumulators are high speed CMOS capable of counter-rates up to 20 megacounts per second and controlled in an accumulation scheme by Main Processor timing.

The high voltage sweeps are controlled either in linear or logarithmic DAC which is controlled by rights either from the DMA ROM or the Main Processor. The entire microprocessor scheme and encoder was built to allow for very fast burst capture of data and to allow intelligent control of events on the spacecraft. An example of this is the Critical Velocity Experiment in which the Main Processor will initiate shape charge ignition via radio control under a controlled condition determined by the locally measured magnetic field.

Science Results

The flight of 38001 was disappointing in that the main scientific goal was not acheived because the two spacecraft were not in the proper orientation. In this experiment, with Gene Wescott of Alaska as the Principal Investigator, we were trying to place two spacecraft on the same magnetic field line at the time of a radial shape-charge ignition. This was not

achieved because one spacecraft severely deviated from our planned trajectory. Some energization of local ions was achieved on the radial shape-charge ignition that did occur from the main instrumentated payload. However, because of the lack of electron data, our science results were very limited. In fact, our main result was the analysis of a previous flight, 34010, very much like this flight, where we did report black holes created in the radial shape-a charge distribution and particles energized in that event.

The Greenland flight was spectacularly successful, in that, due to the simultaneous flight of our vehicle, 29023, and University California, Berkely's vehicle, we did observe simultaneous precipitation of ions from a very far radial distance, as well as, acceleration of electrons simultaneous with the deceleration of protons. These reports are now being worked into a JGR paper. The further use of the very fast burst capture element of our experiment showed, for the very first time, the rapid percipitation of bursts of electrons where we can measure the dispersion in electrons from electrons accelerated a few thousand kilometers above the spacecraft at the nominal altitude of auroral acceleration mechanisms. This is another significant result which we are investigating.

In collaboration with Mike Kelley, we also are investigating the creation of possible kilometric radiation due to the resonant emission of electromagnetic waves along the resonance cone of whistler waves simultaneous with changes in the electron distribution function. In the Critical Velocity Area, our main result has been several papers which have now been published and one soon to be published on the Condor project which occurred before the beginning of this contract, but for which we proposed analysis. The most significant result in that effort has been to point out the discrepancy between our more negative results and those of Project Porcupine reported by Haerendal (1982) in which he reported a large ionization efficiency. Hopefully, the resolution of these descrepancies will occur in the upcoming Crit I launch in May of 1986.

A Magnetospheric Critical Velocity Experiment: Particle Results

R. B. TORBERT and PATRICK T. NEWELL

Center for Astrophysics and Space Sciences, University of California, San Diego

In March of 1983, a barium injection sounding rocket experiment (The Star of Lima) was conducted to investigate Alfvén's critical ionization velocity (CIV) hypothesis in space. Included in the instrumented payload was a UCSD particle detection experiment consisting of five retarding potential analyzers. Despite conditions that appeared to be optimal for the critical velocity effect, the particle data , in agreement with optical observations, indicates that a fractional ionization of only $\sim 5 \times 10^{-4}$ was observed, indicating that the conditions required for the effect to occur are still not well understood. However many of the required phenomena associated with the CIV effect were observed; in particular a superthermal electron population was formed at the expense of ion drift kinetic energy in the presence of intense electrostatic waves near the lower hybrid frequency. The amount of ionization produced is plausibly consistent with the observed electron flux, but could also be accounted for by residual solar UV at the injection point. It is shown based on the UCSD data set that one obvious explanation for the low ionization efficiency, namely that the ionizing superthermal electrons may rapidly escape along field lines, can be ruled out.

I. INTRODUCTION AND EXPERIMENT DESCRIPTION

The critical velocity hypothesis was first advanced by *Alfvén* [1954] in connection with his theory on the origin of the solar system. It states that when a neutral gas moves across magnetic field lines with respect to a plasma with a velocity at least that given by

$$\frac{1}{2} m_n V_c^2 = e\phi_i \qquad (1)$$

where m_n is the neutral mass, and ϕ_i is the ionization potential of the neutrals, a discharge like process can occur which results in the anomalously rapid ionization of the neutrals. The critical ionization velocity (CIV) effect has been reported under a variety of laboratory conditions [for

example, *Piel et al.*, 1980; *Venkataramani and Mattoo*, 1980; *Aznäs*, 1978; *Danielsson and Brenning*, 1975; *Fahleson*, 1961]. The primary evidence for the critical velocity effect occuring in space is a barium injection sounding rocket experiment in the Porcupine series, reported by *Haerendel* [1982]. A comprehensive review of the critical ionization velocity effect in space is given by *Newell* [1985].

The Star of Lima was a conical shaped charge barium injection experiment conducted from Punta Lobos, Peru in March of 1983. The geometry of the experiment is illustrated in Figure 1. The Taurus-Tomahawk rocket had a mother-daughter payload: the explosive charge was separated by spring release from the plasma diagnostics; at detonation the nominal separation was about 2.1 km. The conical charge had an opening full angle of 30 degrees, and it directed the barium beam almost directly across magnetic field lines towards the instrumentation. The launch was just before dawn; the detonation altitude of 429km was calculated to occur below the 3200 Angstrom ionizing uv cutoff, but with sufficient visible sunlight for ground based television observations (calculations by *Wescott et al.* [1986] indicate, however, that the barium cloud was exposed to about 1/40th normal full solar uv). Papers by *Kelley et al.*, [1986]; and *Wescott et al.*, [1986] in this issue discuss the electric and magnetic field data and optical observations respectively. The present work is concerned with the results of the UCSD energetic particle detection experiment.

The energetic particle detector consisted of five retarding potential analyzers (RPAs), a description of which can be found in *Carlson* [1974]. Two sweeping detectors were devoted to ions, two sweeping detectors were devoted to electrons, and one detector measured fixed energy electrons. Table I gives the parameters of interest in the energy sweeps. These detectors exhibit a narrow conical angular response with a half-angle at half maximum of about 3 degrees. The time needed to complete a measurement of an energy spectrum -- 19 ms for the fast electron detector, and 38 ms for all others -- afforded better time resolution than most previous similar particle detection packages.

One of the sweeping electron detectors, and one of the sweeping ion detectors, were tilted at an 8.5 degree angle to the spin axis to give some limited pitch angle information. The three remaining detectors were all oriented along the spin axis, which was vertical to within 10 degrees; and hence nearly perpendicular to the magnetic field lines (refer to Figure 1). These detectors thus had their within 10 degrees of anti-parallel to the ram direction of the barium neutral beam.

Economic constraints dictated a simple, standard design with a comparatively modest dynamic

range of distinguishable particle fluxes. Had the critical velocity effect produced the predicted levels of ionization, all five detectors would have saturated, thereby leaving us with a lower bound on the fluxes. The much lower fluxes observed are reported in the next section.

The plasma parameters of primary interest in the Star of Lima experiment are listed in Table II, along with various other associated quantities which will be useful in later calculations.

II. Results: Data Presentation

The Taurus-Tomahawk rocket overperformed, so that the solar grazing altitude was 41.5km, resulting in the barium cloud being exposed to 1/40th the normal ionizing efficiency of full uv. The total amount of vaporized barium released in the burst was of the order 10^{24} atoms; the amount of barium ionized is estimated from the brightness of the BaII 4554A line observed by ground stations to be 5×10^{20} ions [*Wescott et al.*, 1985]. This is about 1/40th the amount normally observed in a similar release exposed to full sunlight. The uncertainties are large enough that the precise agreement must be accidental, but it is clear that solar uv is at least potentially capable of accounting for all the ionization that occurred. However, it is also true that electron impact ionization, in accordance with the critical velocity effect, could have caused as much ionization,as is shown below. Moreover, a wealth of plasma phenomena was observed, giving insight into the processes in effect.

Figure 2 shows the electron data near the explosion, which occurred near 340.65 s flight time. The Cornell quasi-dc electric field (single-axis double-probe, not despun) measurements are included for reference. The ion data is given in Figure 3, which is on the same time scale, and includes pitch angle information. Note that the "90 degree" electron sweeping detector saturated (while sweeping through the lowest energy step) and took approximately one second to recover. All other detectors appeared to always have dynamic range in reserve; some, particularly the "80 ion rpa" (tilted at an 8.5 degree angle to the spin axis) obviously never came near saturation. Thus the flux rates reported here are believed to be reliable to within a factor of about 3 (the uncertainty arising mostly from uncertainty in the energy acceptance widths). A chronology of the effects seen by the *in situ* diagnostics is given first to provide an overview.

The ground based television cameras can determine the explosion time to about a single frame (1/60 s) resolution. Unfortunately, the time recording on the tapes was hand calibrated, so that it cannot be used for a reliable determination of the explosion time. The highest gain channel on the Cornell electric field experiment provides the best estimate of the detonation

time. Prior to the arrival of any particles, with their associated strong wave activity, a 10 ms precursor electric field pulse of amplitude $50\mu V/m$ was detected. This is very likely a magnetosonic wave, which -- moving at the Alfvén speed -- would be the fastest traveling plasma disturbance created by the explosion. This precursor wave arrived at the payload at flight time 340.658 s. The time of flight of a magnetosonic wave to the payload would only be ~3 ms. It is not clear how long after detonation such a wave would be emitted; however we may take 340.658 as the approximate explosion time. For convenience, events in the Star of Lima experiment will be hereafter be referred to in burst time, where the origin in burst time corresponds to 340.658 flight time (21 March 1983 09:58:24.658 UT).

Figure 4 shows .6 sec of energetic ion and electron data following the explosion on an expanded time scale. The analyzing sweep voltage is included in the top panel, with the lowest energies in the electrons in panel 2 corresponding to minima in this waveform. (Refer to Table I for sweep ranges). Starting at ~62 ms burst time, the first superthermal electrons were observed, along with the onset of the oxygen lower hybrid waves (not shown) as reported by *Kelley et al.* [this issue]. Note that counts appear first only in the lowest end of the energy sweep; within a few tens of milliseconds the electron tail population heats up (the flux versus energy profile broadens). This is the pattern one would expect for electrons heated by local wave instabilities. Electrons energized elsewhere would show the inverse dispersion pattern: the most energetic electrons would appear first. At 82 ms burst time the first energetic ions were observed. Five milliseconds later, the biggest electric field event of the flight occurred; a large dc electric field pulse of at least 400mv/m amplitude. Because the orientation of the electric field with respect to the single axis of the electric field boom is unknown, this figure is a lower limit on the field strength.

To have reached the payload by this time, neutrals would be required to have a velocity of a little greater that 20 km/sec, which, in fact, corresponds to an electric field of 440 mv/meter, consistent with that observed. However, *Wescott et al.*, [this issue] report no barium ions with velocities greater that 14 km/sec. In fact, using their velocity profile, one can show that the barium density begins to rise at the payload at about 160 ms burst time and reaches a peak of about $2\times10^8/cm^3$ at 220 ms, all after this main electric field pulse, but corresponding precisely to the times of maximum barium lower hybrid,as later described. Presumably,then, this dc pulse is associated with the arrival of either ambient neutrals pushed ahead of the main barium jet or some contaminent of the barium which has never been seen before. To our knowledge, no diagnostic payload has ever been in the main jet of such a shaped charge. It is indicative that

the primary wave spectrum at this time is more characteristic of oxygen than barium. In any event, these early waves do heat the electrons and begin to ionize whatever neutrals are present. This may in turn cause a strong electric field to be set up in the beam direction to hold back the unmagnetized ions and subsequent polarization of region. The observed electric field could then be explained. However, it seems odd to us that beam neutrals at this time, undoubtedly of much lower density than at later times, have such a large effect in accelerating the entire background population up to 20 km/sec. Without a full three-dimensional measurement of the electric field, the interpretation of the pulse thus remains unresolved.

Starting at about 150 ms burst time, broad band electrostatic oscillations with a high frequency cutoff at the barium lower hybrid frequency are observed. A power spectrum of these oscillations and a detailed discussion is found in *Kelley et al.*, [1986]. For reference, the local beam neutral density begins rapidly to rise at 160 ms, exceeds the ambient at 170 ms, reaches a peak of 2×10^8 /cm^3 at 230 ms, and decays to a low level (1×10^7) by 350 ms. As will be discussed in detail below, these times and those of the oscillations correspond also to the time that the electron energy flux is gaining energy at the expense of the ion kinetic energy. Note the rapid appearance of the peak in the electron spectrum at 165 ms in panel 2 of figure 4. By ~260 ms burst time the oscillations have largely died away. After about 300 ms the ions have ceased to lose energy, and the electrons to gain energy. Thereafter, the electron population cools, while the ions flux remains stable. The electron population remains isotropic until about 400 ms burst time. Thereafter a strong loss cone distribution forms in the electrons.

The absolute value of the ion flux rates can be used to estimate a percentage ionization. The peak flux rate, occurring at 242 ms burst time, was about 3×10^{10} ions/cm ^{2}-s-str implying ion densities on the order of 5×10^4/cm^3. Using the above neutral cloud density, the ionization at the time the cloud passed over the instrumented payload can can be readily calculed to be a little more than 10^{-4}.

A 10 km/s barium atom (a typical value for this type shaped charge) had a gyroradi of 650m for our value of magnetic field strength (.22gauss). Since the separation from the explosion point was ~2km, we would presumably observe little of the initial thermal ionization; or indeed, any ionization which occurred more than a km away from the instrumented payload. Thus any ionization which occurred after the cloud passed over the payload would not be detected. In this light, it is appropriate to report dn_i/dt; in effect the number of ions observed divided by the time the cloud spent within a gyroradi of the payload. Taking, say, a 14 km/s leading edge, and a 3 km/s trailing edge one obtains $dn_i/dt \approx 10^5$ /cm ^{3}-sec. This rate of ion production gives

a total ionization efficiency (a few times 10^{-4}) that is consistent with the optical observations and is three orders of magnitude below the value reported for Porcupine [Haerendel,1982].

Electron heating, resulting in a superthermal electron tail, has undoubtedly been observed. The peak flux in electrons was about 5×10^{10}/cm^2-sec-str, which leads to an estimate of the density of superthermal electrons of ~500/cm^3 with energy greater than about 7 ev. Photoelectrons are much too cold to account for the energetic electron population observed; only collective plasma processes could produce the heating that occurred. In particular, there is a clear association of the energetic electrons with rapid electric field oscillations.

The cross section for electrons to ionize barium is crudely a step function, with the value 1.0 to 1.2×10^{-15}cm^2 above 7 ev, and 0 below 7 ev [*Vainshtein, et al.*, 1972]. The amount of ionization the observed number of superthermal electrons would be expected to create is readily calculated:

$$\frac{dn_i}{dt} = n_e\, n_n \sigma\, v_e \qquad (2)$$

where $\sigma = 1\times10^{-15}$cm^2; $v_e = 2\times10^8$ cm/sec is a typical (10 ev) electron velocity; n_e is the superthermal electron tail density; and n_n is the density of neutral barium. One finds $dn_i/dt = 3\times10^4$/cm^3-sec. This is reasonably consistent with (but somewhat lower than) the rate of ion production actually observed as the cloud passed over the payload.

Figures 5 and 6 show ion and electron energy flux spectra during the event. Each spectrum consists of a single upsweep of either the "80 degree" e- or the "90" ion RPA. Of course, other spectra are also available and have been made from the downsweep and from other detectors as well, but to facilitate easy comparison -- especially of the quantitative values obtained by integrating these curves Table III -- it is desirable to minimize extraneous variations. The upsweep is preferred for generating spectra to the downsweep since a wider energy range is covered. The detectors chosen had the best coverage (for example, the fast electron detector died and hence is unsuitable for the present purposes).

The earliest ion spectrum -- the first for which count rates were significant -- is contained in Figure 5, 78 ms after the explosion. This first spectrum has the appearance of a drift maxwellian with a peak around the retarding potential of 25 ev (implying about a 30 or 35 ev actual ion energy peak). The second spectrum contained in this figure, taken at 155 ms, shows that the peak has shifted to lower energies. Since there has been further ionization, there are more ions around at all energies. However it is clear that individual ions are losing energy; and the shift

is far too rapid to be accounted for by dispersion alone. Since this is accompanied by the rise of electrostatic fields and heating of electrons, it is clear that a collective plasma process is underway transferring kinetic energy from the ions to the electrons.

The next panel of Figure 5 shows that by 232 ms burst time, the ion distribution has relaxed, and lost much of the beam-like form that characterized it earlier. By this time the electron heating is well under way. Notice again the shift of the distribution towards fewer ions at high energy and more at lower energies.

Piel et al. [1980] have argued for the importance in laboratory experiments of an inhomogeneous ionization front. Although it appears that such a front could have passed over the payload, beginning at about 150 ms burst time and ending around 260 ms burst time, this time history can also be acounted for by the simple variation of the driving beam density as discussed above. These time variations are also seen in the abrupt drop in ion density observed between the spectrum beginning at 232 ms and the spectrum starting at 309 ms (refer to Figure 5). Thereafter the ion distribution is very stable on the time scale of interest here. For example, Figure 5 shows that there is essentially no change in the ion flux distribution between 309 ms burst time and 693 ms. All intervening ion spectra are essentially identical and so are not shown here.

The electron spectra show less consistency than the ion spectra, but the general trends are clear. Shortly after 100 ms a superthermal electron population begins to form. Figure 6 shows first the electrons at 232 ms burst time, and reaching their peak at 309 ms. Although the ions experience a sharp drop off at this time, the electrons do not: Figure 6 shows the electrons are still at peak energy flux as late as 386 ms. Thereafter the electron flux does begin to drop, however, and as the final panel of Figure 6 illustrates, the electron energy flux is much reduced by 463 ms burst time.

Some sample energy fluxes and densities calculated by integrating these curves are summarized in Table III. In computing these values, the ion distribution was assumed to be extended over one ster-radian, and the electrons over 4π ster-radians (in accordance with the apparent isotropy of the electrons as discussed below, and the observed strong anisotropy in the ion distribution).

Figure 7 gives some limited insight into the pitch angle dependence of the energetic electron population. The plots in this figure are generated from the RPA which was devoted to electrons and which was tilted at an 8.5 degree angle to the spin axis. Thus it spun through about a 17 degree range of pitch angles. The detector was sweeping in energy; therefore the data in

Figure 7 is a subset, each panel corresponding to a given energy level. Note that for approximately 0.4 seconds the population is apparently isotropic (or at least flat near 90 degrees). This is the time of peak electric field fluctuations, and also the time of peak particle fluxes. Thereafter the population becomes sharply peaked, as all electrons not very near 90 degrees quickly escape along field lines. At these later times, the ratio of the population near 90 to that at about 70 is roughly 30:1. We will return later to the significance of the initial isotropic phase.

III. Discussion

The data shows that the phenomena associated with the critical velocity effect -- namely heating of the electrons at the expense of ion kinetic energy, and associated broad band electric waves around the lower hybrid frequency -- were indeed observed. The process failed to build on itself in a rapid non-linear fashion; i.e., it did not reach discharge. This is something of a puzzle when contrasted with the results of Porcupine, a similar barium injection experiment in which nearly 30% ionization efficiency was reported [*Haerendel*, 1982].

A number of possible reasons for the low ionization efficiency ($\sim 5 \times 10^{-4}$) observed in the present experiment can be advanced. To discuss all of these in any detail is beyond the scope of the present work (an article discussing many of the possibilities in detail is in preparation). However our data provides considerable evidence concerning one apparent difficulty: the rapid escape of the superthermal electrons along the magnetic field lines.

For the critical velocity effect to be viable, it is clearly necessary that a newly energized superthermal electron have time to have at least one ionizing collision during the course of the process. Thus, in analogy with the Townsend condition for beam plasma discharges, *Brenning* [1982] has introduced the requirement:

$$\tau_p > \tau_H + \tau_{ion} \tag{3}$$

where τ_p is the time over which CIV effects occur, τ_H is the energization time for a superthermal electron, and τ_{ion} is the time it takes such an electron to have an ionizing collision with a neutral. Because of the rapid time scale for the lower hybrid instability, it is probably safe to take the energization time, τ_H, to be much shorter than the other times of interest.

The time it takes an electron to have an ionizing collision is readily calculated:

$$\tau_{ion}(v) = \frac{1}{n_n \sigma_{ion}(v)\, v} \approx 25 \text{ ms} \qquad (4)$$

where the cross section [*Vainshtein et al.*, 1972] and velocity used were those appropriate to a 10 ev electron; and the neutral barium density was taken to be $2\times10^6/\text{cm}^3$. The time available for the CIV process to grow to discharge is not well defined, but is of the order of the "contact time" that fast flowing neutrals spend on a given field line. This is hundreds of milliseconds, clearly much longer than the necessary 25. Thus the Townsend condition in this sense appears satisfied.

From equation (2), it is clear that this τ_{ion} is also the time scale for the growth of the plasma density, which is essentially independent of how rapidly the electrons are heated. Their energy is fixed by a resonance condition with the wave. One could argue that, given only 200 ms of "contact time," the density at the payload could only increase by a factor of a few hundred. However, this would not explain the absence of ionization at, say, 6 km from the explosion, where the time scales are 3 times as long. At these distances, Porcupine produced its maximum ionization [Haerendel,1982].

There is also, however, the question of electron containment. A 10 ev superthermal electron has a velocity of 2000 km/s, and hence could escape in a fraction of a millisecond from the cloud, which has a length parallel to B of only ~600 meters. Thus the escape time appears to be much more rapid than the ionization time, which would suppress CIV effects. Now such an escape current would tend very rapidly to build up a containing electric field; the question is whether the background plasma -- which has an electron density much larger than the superthermal electron density -- would rapidly short out any such polarization field parallel to B. It will now be shown that our experimental data shows that the electrons were indeed trapped for much longer than the nominal escape time.

Refer to Figure 7, which illustrates the dependence of flux rates on pitch angle at various fixed energies. Notice that during the time of peak flux rates, say the .3 sec starting at burst time 92 ms, the electron distribution appears to be independent of pitch angle. This is not, of course, to say that the flux rates are constant during this interval: indeed there is time dependence as is discussed in detail in the previous section. However the fluxes appear to have no dependence on pitch angle during this time period.

At a somewhat longer time a marked loss cone distribution emerges. Indeed, after say 600 ms burst time, the ratio of the flux near 90 to that at about 75 degrees is (with appreciable variation) around 30:1. This, however, happens on a time scale much longer than CIV processes could possibly be operative. Thus the pitch angle data indicates that the hot electrons are contained, at least for a much longer time scale than the fraction of a millisecond nominal escape time.

It may be suggested that the electrons are being energized primarily along the field lines, as well as escaping along them, in such a way that the observed isotropy is produced. It is *a priori* unlikely that these effects could balance so closely. Furthermore, there is a compelling argument based on energy considerations which shows explicitly that such a coincidence is not occurring.

Refer to Table III. This table shows the ions initially losing kinetic energy, and the electrons heating up. Note that the energy density of the ions is at all times much larger than the energy density of the electrons. However the electron energy flux is much higher than the ion energy flux; indeed, by burst time 386 ms, the electron energy flux is 2.4×10^{12}ev/sec-cm^2, whereas the ion energy flux is only 5.7 $\times10^{10}$ev/sec-cm^2. This is not surprising, since for a given energy density, the much lighter mass of the electrons implies a much higher energy flux. The point is that these differences in energy flux could not be maintained if the electrons were escaping along field lines.

To conserve energy, it is clear that the electron energy flux escaping along field lines can only be a fraction of the ion energy flux into the region perpendicular to B. Unfortunately it is not possible merely from the observations of total net flux to deconvolve the sinks and sources. To be more explicit: the ion flux, for example, is increased by new ionization, and decreased by dispersion as well as by energy transfer from the ions to the electrons. Nonetheless, it is an observational fact that large numbers of ion are not being created, which allows a very rough estimate of the electron trapping time -- which will be denoted τ_T -- as follows. The physical quantity which most closely corresponds to the detector count rate is the electron energy flux, j_{Ee}. Imagine, a box of width w perpendicular to the beam direction and arbitrary lengths in the other two dimensions. At any instant of time, the electron energy flux out of the sides of this box along B is proportional to j_{Ee} . If the electrons are trapped, this energy loss is reduced by the ratio of the un-impeded electron transit time τ_{free} to the trapping time. This τ_{free} is essentially the length w divided by a typical electron velocity. Now, the upper limit to the energy available in this box is given by the difference between the ion energy flux (j_{Ei}) which is

flowing in and that which is flowing out the other side. Setting this value as a maximum, we arrive at:

$$\frac{\tau_T}{\tau_{free}} > \approx \frac{2 j_{Ee}}{w\left(\frac{\partial j_{Ei}}{\partial r}\right)} \tag{5}$$

where the derivative of j_{Ei} is taken along the beam direction. The maximum value of this derivative is certainly given by dropping the entire value of j_{Ei} over one ion gyroradii, about the value of w at the location of the spacecraft. Using the values in Table III at 386 ms for j_{Ee} and j_{Ei}, and a value of about 0.3 ms for τ_{free}, we find that the trapping time is greater than about 25 ms. This estimate is obviously very crude, but is remarkably consistent with the ionization time given in equation 4. In fact, τ_T is really an *energy* trapping time and should never be greater than the ionization time for weakly ionizing discharges. Thus, the effects of electron escape appear to be no greater than the damping effect of energy loss due to the ionization process itself. The present arguments make clear that energy conservation requires a trapping time orders of magnitude larger than the nominal fraction of a millisecond escape time the electrons would have if they were uncontained.

Thus both the energetics of the observed particle distributions, and the isotropy of the electron distribution demonstrate that the superthermal electron population is contained for far longer than the nominal escape time.

IV. Summary and Conclusions

An energetic (1-50 ev) particle detection experiment was designed and built for inclusion on the Star of Lima, the first sounding rocket experiment intended solely to test the critical velocity effect in space. The results of the experiment were negative, in that the ionization efficiency from superthermal electron impact was quite low ($\approx 5\times10^{-4}$ fractional efficiency). However, a detailed analysis of the particle data demonstrates some important results. As required by all critical ionization velocity theories, superthermal electron tail formation was observed. In accordance with predictions by prevailing theories, this was accompanied by

broadband electrostatic oscillations near the barium lower hybrid frequency and a demonstrable energy loss in the ion spectrum. There is thus no doubt that the electrons were energized by a collective plasma process at the expense of the ion drift kinetic energy. Thus some of the essential features of the CIV mechanism were directly measured. Analysis of this data puts constraints on speculations into why the CIV operated at such a low level.

The most important example of this is that the superthermal electrons were trapped for far longer than their nominal escape time. The pitch angle isotropy observed, as evidenced by Figure 7 suggests such a containment. Energy conservation arguements based on the measured fluxes demonstrate convincingly that this is so. Thus one important possible explanation for the observed low efficiency is eliminated.

The experiment described in this paper was performed under conditions which would ordinarily be expected to maximize CIV effects, and yet only a very low ionization efficiency was observed. It is thus established that the counterstreaming of a plasma and a neutral gas in a space environment does not necessarily lead to CIV effects.

In view of the large number of proposed applications for the critical velocity effect in space [*Newell,* 1985] it is of considerable practical importance -- as well as being of intrinsic fundamental interest -- to resolve the question of when to expect CIV effects in space. Further magnetospheric barium injection experiments remain the most promising means of resolving the issue.

Acknowledgements. This work was supported by the NASA grants NAG 5-610 and NGL-05-005-007.

References

Alfvén, H., *On the Origin of the Solar System*, Oxford at the Clarendon Press, London, 1954.

Axnäs, I., Experimental investigation of the critical ionization velocity in gas mixtures, *Astrophys. Space Sci., 55*, 139-146, 1978.

Brenning, N., Comment on the Townsend Condition, Workshop on Alfven's Critical Velocity Effect,Garching,Munchen,October 11-13,1982,pp. 313-320.

Carlson, C., Rocket measurements of auroral zone low energy charged particles, Ph.D. dissertation, University of California, Berkeley, 1974.

Danielsson, L. and N. Brenning, Experiment on the interaction between a plasma and a neutral gas. II, *Phys. Fluids, 18*, 661-671, 1975.

Fahleson, U., Experiments with plasma moving through neutral gas, *Phys Fluids, 4*, 123-127, 1961.

Haerendel, G., Alfvén's critical velocity effect tested in space, *Z. Naturforsch. A 37*, 728-735, 1982.

Kelley, M. C., R. Pfaff, G. Haerendel, Quasi-dc and wave electric field measurements in the CONDOR critical velocity experiment, *J. Geophys. Res.*, this issue.

Mcbride J. B., E. Ott, J. P. Boris, and J. H. Orens, Theory and simulation of turbulent heating by the modified two-stream instability, *Phys. Fluids, 15*, 2367-2383, 1972.

Newell, P. T., Review of the critical ionization velocity effect in space, *Reviews of Geophysics*, (in press).

Piel, A., E. Möbius, and G. Himmel, The influence of the plasma inhomogeneity on the critical velocity phenomenon, *Astrophys. Space Sci., 72*, 211-221, 1980.

Sherman, J. C., The critical velocity of gas-plasma interactions and its possible hetegonic relevance, Nobel. Symp. No. 21, edited by Almqvist and Wiksell, Uppsala, p. 315, 1972.

Vainshtein, L. A., V. I. Ochkur, V. I. Rakhovskii, and A. M. Stepanov, Absolute values of electron impact ionization cross sections for magnesium, calcium, strontium and barium, *Sov. Phys. JETP Engl. Transl., 34*, 271-275, 1972.

Venkataramani, N., and S. K. Mattoo, Plasma retardation in Alfvén's critical velocity phenomena, *Physics Letters 79A*, 393-398, 1980.

Wescott, E. M., G. Haerendel, M. C. Kelley, and R. B. Torbert, Star of Lima, Star of Condor: Two rocketborne Alfén critical velocity experiments, this issue.

P.T. Newell and R.B. Torbert, Center for Astrophysics and Space Sciences, University of California, San Diego, La Jolla,

CA 92093.

Figure Captions

Figure 1. Geometry illustrating the Star of Lima barium injection experiment. The arrows pointing out of the instrumented payload show the direction of the "90" and "80" degree RPAs.

Figure 2. Electron differential energy fluxes near the explosion (t= 0). The Cornell electric field data (not despun) is shown for reference.

Figure 3. Ion differential energy fluxes near the explosion.

Figure 4. The electron data near the explosion on an expanded time scale. Again Cornell electric field data is included for comparison (refer to *Kelley, et al.*, this issue).

Figure 5. Ion differential energy flux as a function of energy at selected times. Each curve is based on the data from one upsweep of the "90 degree" ion detector (which took 38 ms to complete). The times given are the burst time at which the sweep was started.

Figure 6. Electron differential energy flux as a function of energy at selected times. Each curve is based on the data from one upsweep of the "80 degree" electron detector (which took 38 ms to complete). The times given are the burst time at which the sweep was started.

Figure 7. Electron differential energy fluxes at specified energies (6-11.4 ev) for the "80 degree" detector. The actual pitch angle is also plotted. Note the period of approximate isotropy during the time of peak fluxes (the lower energy electrons are becoming more numerous during this time period).

Table Captions

Table I. Characterizing the energy sweeps of the retarding potential analyzers. "Accum" is the accumulation time at a single energy step, and "Spectrum" is the time needed to complete one upsweep or downsweep.

Table II. Important parameters and typical values for the Star of Lima experiment.

Table III. Energy densities and fluxes for superthermal electrons and ions at times near the burst. Values are obtained by integrating the area under curves such as those shown in figures 5 and 6.

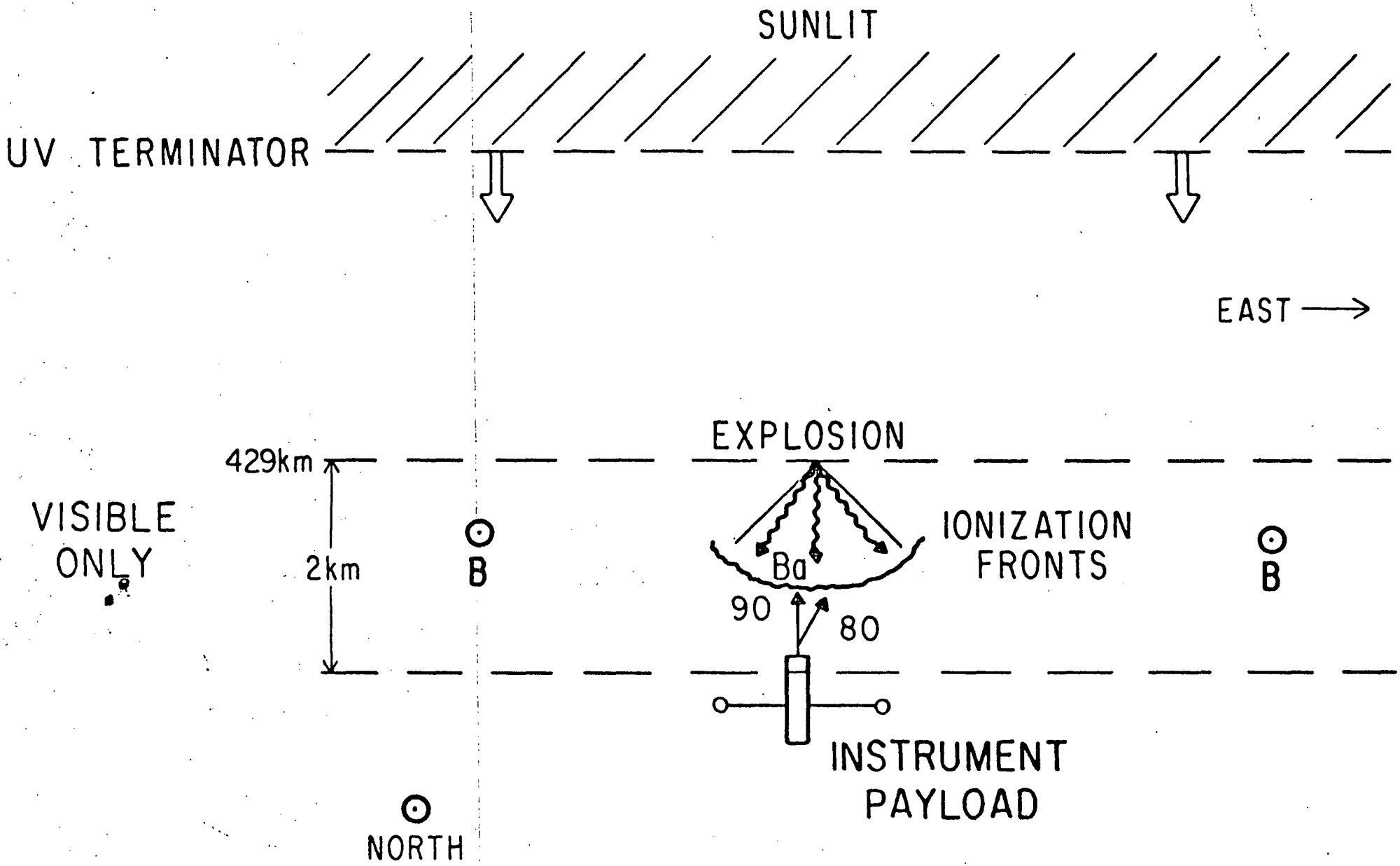

CRITICAL VELOCITY EXPERIMENT OVER CHILCA, PERU

Fig. 1

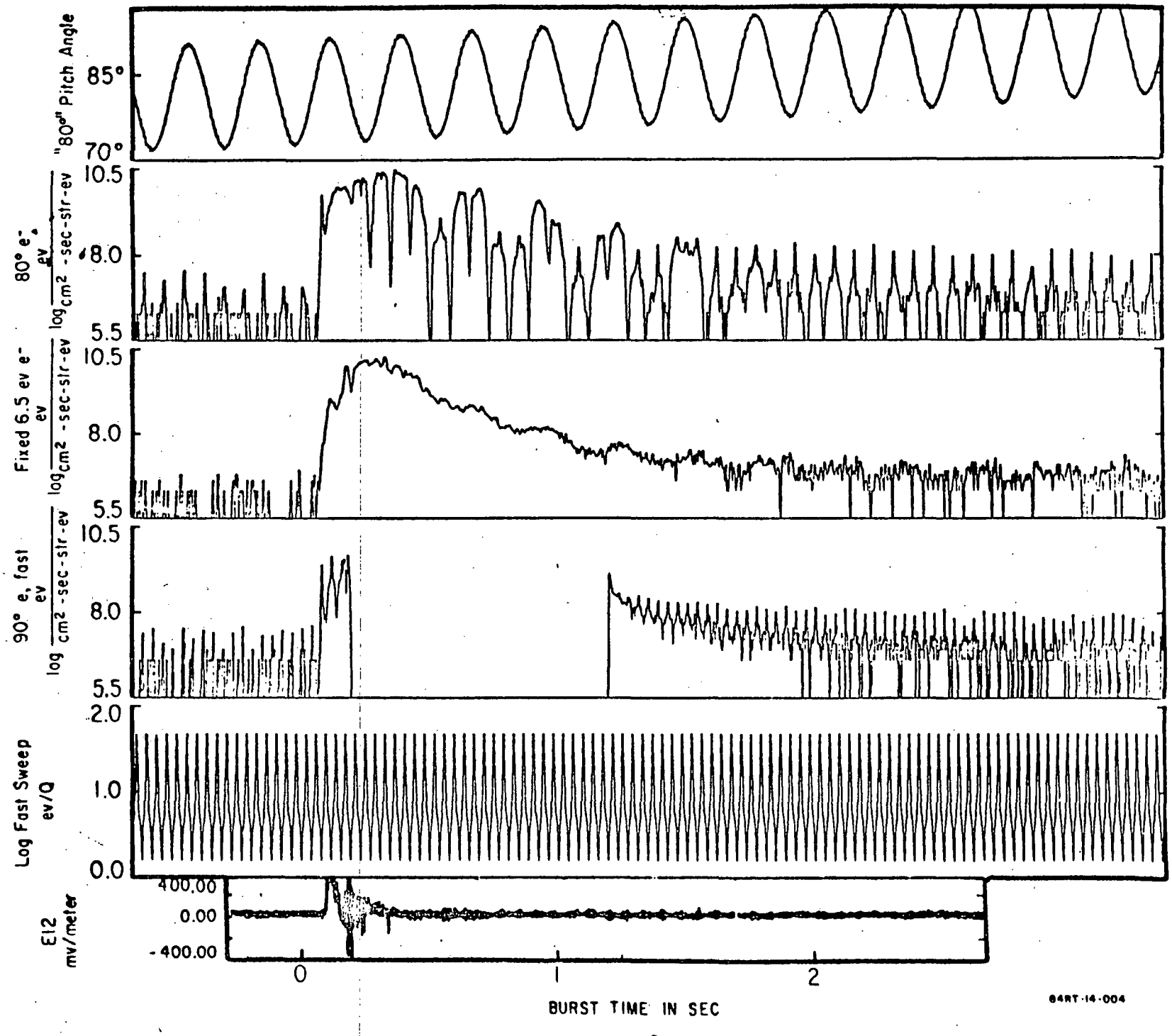
ELECTRON DIFFERENTIAL ENERGY FLUXES
"80°" Pitch Angle
85°
70°
80° e⁻, ev
log cm² -sec-str-ev
10.5
8.0
5.5
Fixed 6.5 ev e⁻
ev
log cm² -sec-str-ev
10.5
8.0
5.5
90° e, fast
ev
log cm² -sec-str-ev
10.5
8.0
5.5
Log Fast Sweep
ev/Q
2.0
1.0
0.0
E12
mv/meter
400.00
0.00
-400.00
0
1
2
BURST TIME IN SEC
64RT-14-004

Fig. 2

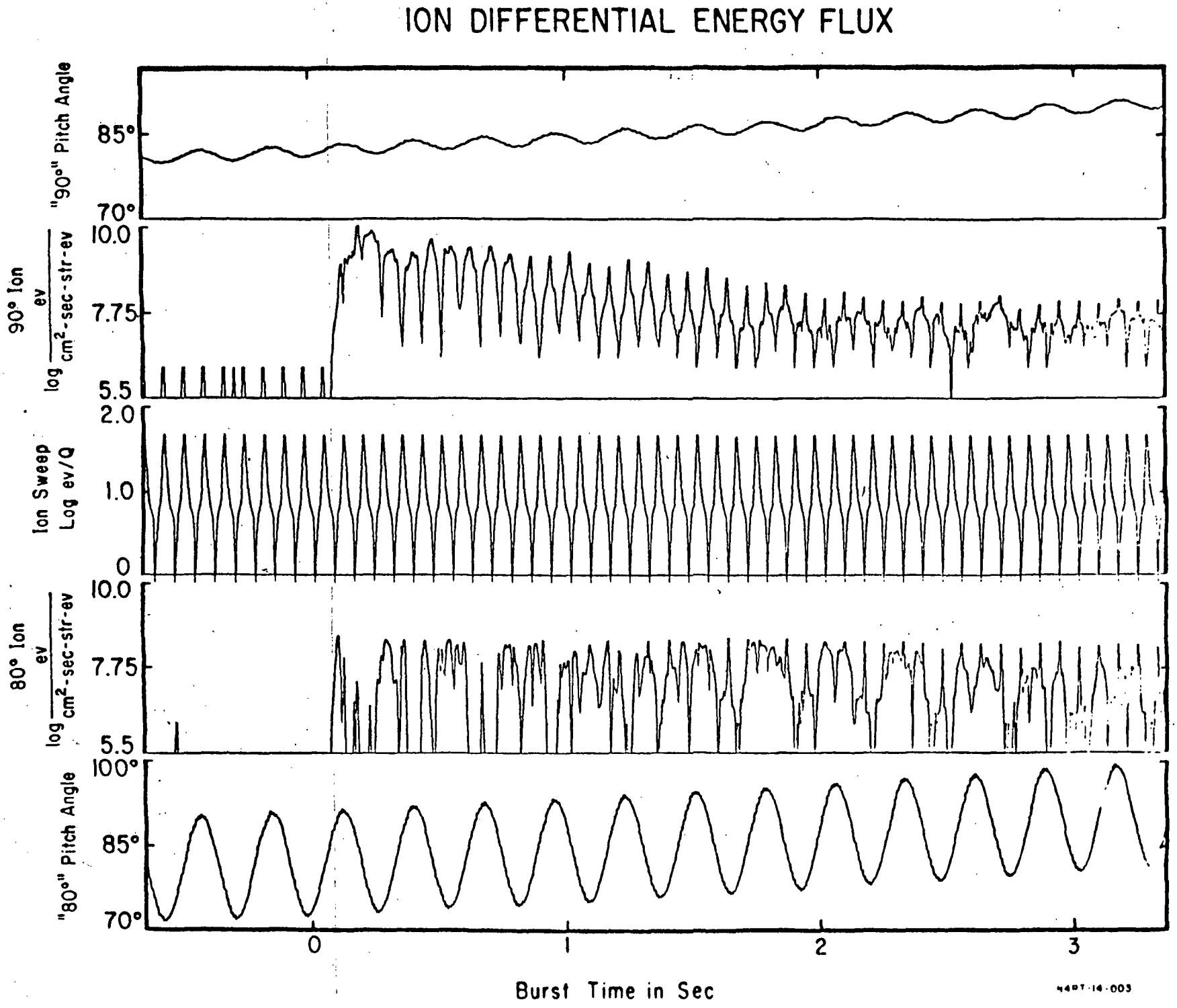
ION DIFFERENTIAL ENERGY FLUX
"90°" Pitch Angle
85°
70°
90° Ion ev / log cm²-sec-str-ev
10.0
7.75
5.5
Ion Sweep Log ev/Q
2.0
1.0
0
80° Ion ev / log cm²-sec-str-ev
10.0
7.75
5.5
"80°" Pitch Angle
100°
85°
70°
0
1
2
3
Burst Time in Sec
44PT-14-003

Fig. 3

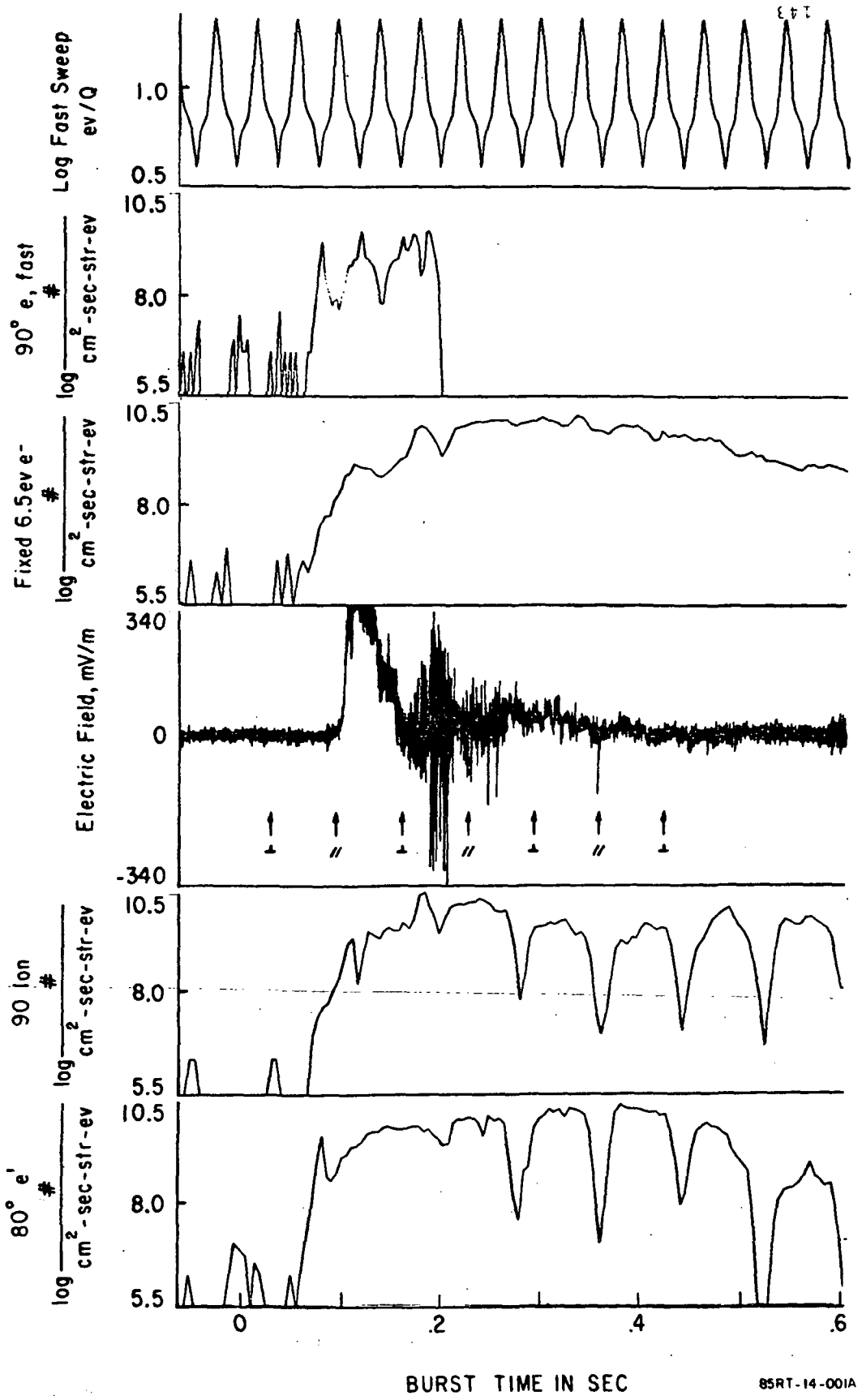
Log Fast Sweep ev/Q
1.0
0.5
90° e, fast
log # / cm²-sec-str-ev
10.5
8.0
5.5
Fixed 6.5ev e⁻
log # / cm²-sec-str-ev
10.5
8.0
5.5
Electric Field, mV/m
340
0
-340
90 Ion
log # / cm²-sec-str-ev
10.5
8.0
5.5
80° e'
log # / cm²-sec-str-ev
10.5
8.0
5.5
0
.2
.4
.6
BURST TIME IN SEC
85RT-14-001A

Fig. 4

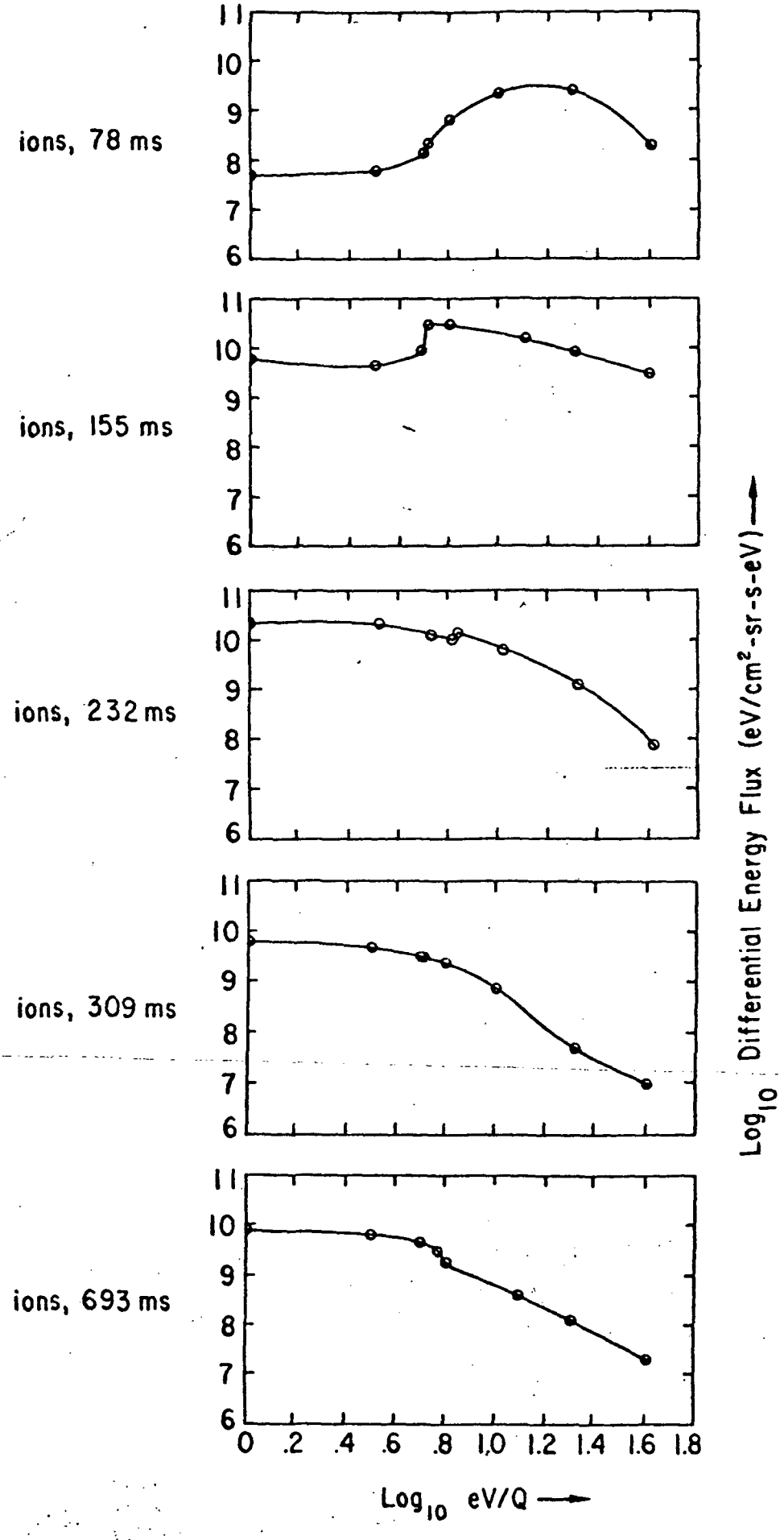
ions, 78 ms
ions, 155 ms
ions, 232 ms
ions, 309 ms
ions, 693 ms
11
10
9
8
7
6
0 .2 .4 .6 .8 1.0 1.2 1.4 1.6 1.8
Log10 eV/Q
Log10 Differential Energy Flux (eV/cm²-sr-s-eV)

Fig. 5

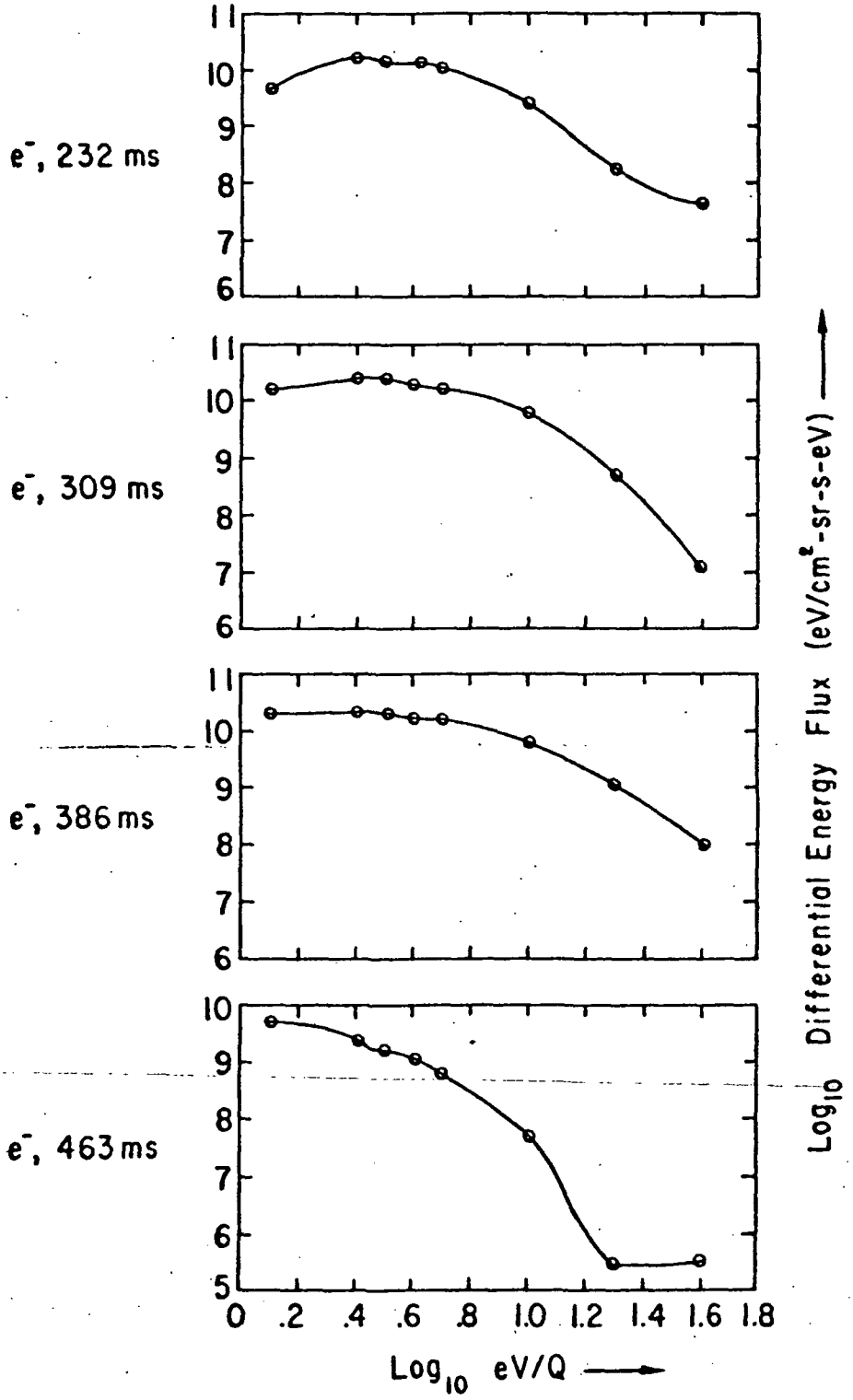
e⁻, 232 ms
e⁻, 309 ms
e⁻, 386 ms
e⁻, 463 ms
11
10
9
8
7
6
5
0
.2
.4
.6
.8
1.0
1.2
1.4
1.6
1.8
Log10 eV/Q
Log10 Differential Energy Flux (eV/cm²-sr-s-eV)

Fig. 6

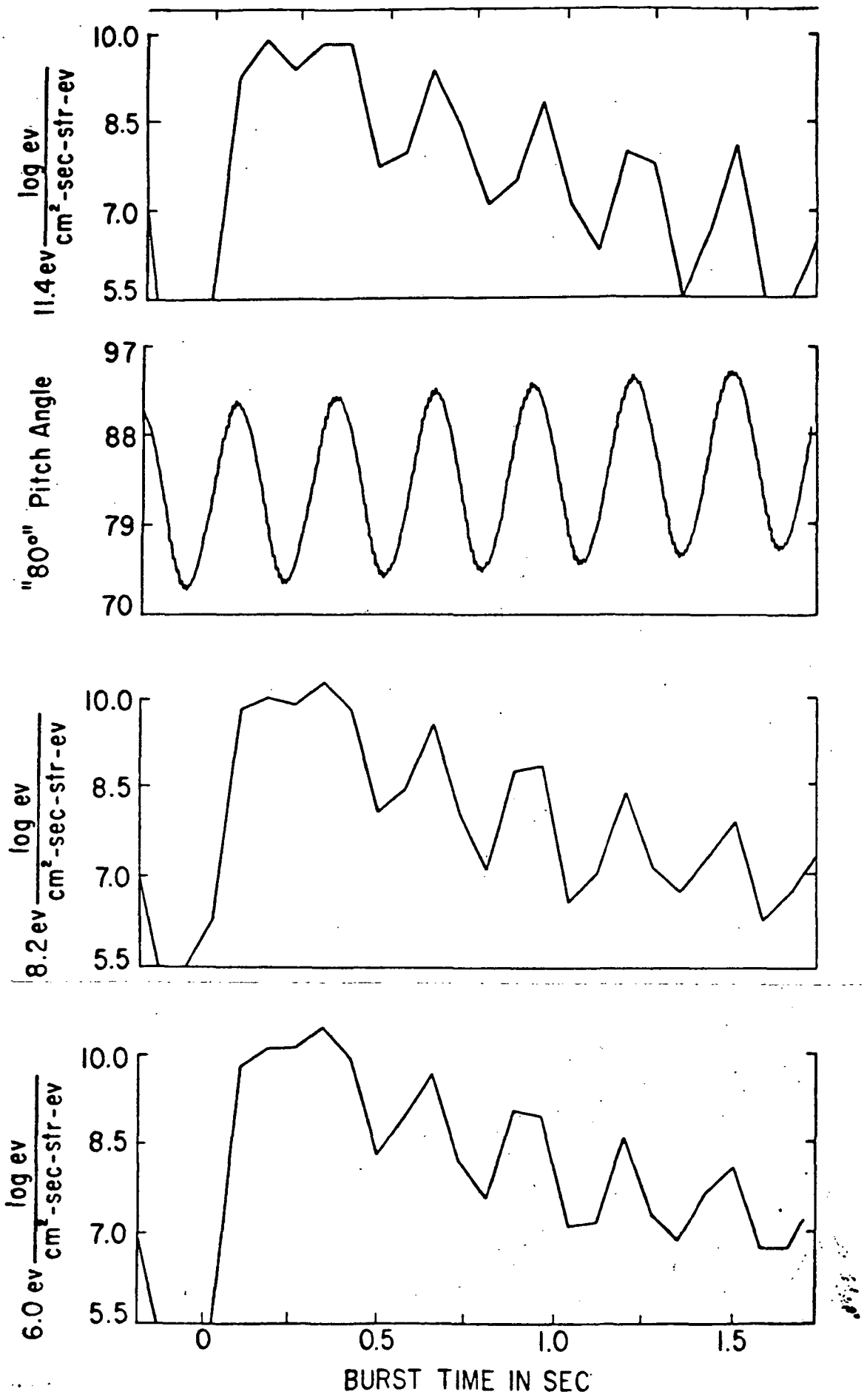
10.0
8.5
7.0
5.5
11.4 ev log ev / cm²-sec-str-ev
97
88
79
70
"80°" Pitch Angle
10.0
8.5
7.0
5.5
8.2 ev log ev / cm²-sec-str-ev
10.0
8.5
7.0
5.5
6.0 ev log ev / cm²-sec-str-ev
0
0.5
1.0
1.5
BURST TIME IN SEC

Fig. 7

Table I. RPA Sweep Parameters				
Particles	Angle	Accum (msec)	Spectrum (msec)	Energies (ev)
e-	" 90 "	2.40	19.2	1.5-47
e-	" 90 "	4.80	--	6.5
e-	" 80 "	4.80	38.4	1.5-48
ions	" 90 "	4.80	38.4	.8-47
ions	" 80 "	4.80	38.4	.8-46

Table II. Star of Lima Plasma and Particle Parameters	
Altitude	428km
Background plasma density	n = 2 or 3 $\times 10^4/cm^3$
Background neutral density	$n_o = 6.7 \times 10^7/cm^3$
Magnetic field	B = .22 gauss
Debye length	$\lambda_D = 2cm$
Typical Ion gyroradius	ρ_i (Ba, 10km/sec)=650m
Typical e- gyroradius	ρ_e (10ev) = 52cm
Ion gyrofrequency	ω_{ci} (Ba) = 15.3 rad/sec
Electron gyrofrequency	$\omega_{ce} = 3.87 \times 10^6$rad/sec
Plasma frequency	$\omega_{pe} = 9 \times 10^6$rad/sec
Ba Ion Plasma frequency	$\omega_{pi} = 1.8 \times 10^4$rad/sec
Lower hybrid frequency	$\omega_{LH} = 6.5 \times 10^5$ rad/sec
Alfven velocity (O)	$v_A = 700$ km/sec
Particle/Field pressure	$\beta \approx 2 \times 10^{-5}$

Table III. Selected Energy Densities and Fluxes				
Time	Flux (10^{12}ev/sec-cm^2)		Density (kev/cm^3)	
msec	e-	ions	e-	ions
78	1.4	.063	5.8	123
155	3.8	.45	17	1151
232	1.2	.21	9.5	792
309	2.4	.041	18	182
386	2.4	.057	18	223
463	.14	.054	1.5	272
693	.33	.042	3.2	200

BLACK HOLES, WAVES, AND ENERGIZED PARTICLES FROM HIGH ALTITUDE EXPLOSIVE PLASMA PERTURBATION EXPERIMENTS

by

E. M. Wescott, H. C. Stenbaek-Nielsen, T. Hallinan,
C. Deehr, J. Romick, and J. Olson
Geophysical Institute, Fairbanks, Alaska
AM841926
Alaska Univ

M. C. Kelley and R. Pfaff
Cornell University
C5729333
Ithaca

R. B. Torbert and P. Newell
University of California at San Diego
CD305309

H. Föppl
Max Planck Institut für Extraterrestrische Physik
MM602008
Garching

J. Fedder
Naval Research Laboratory
NS999791

H. Mitchell
IRT Corporation
I5099092

ABSTRACT

High explosive shaped charge experiments King Crab, Bubble Machine I and II, designed to perturb the ambient plasma and magnetic field were flown above 460 km on Taurus Tomahawk rockets from Poker Flat in March 1980, 1981 and 1982, repectively. The last two flights were a mother-daughter combination with the instrumentation section remaining attached to the rocket. Cornell University furnished a single axis dipole electric field detector, and a fixed bias cylindrical Langmuir probe. A three axis attitude magnetometer was also flown. The University of California at San Diego furnished a curved plate energetic ion and electron electrostatic analyzer.

The first experiment, King Crab, revealed the existence of a barium plasma depleted region or black hole of about 5 km diameter centered on the burst. All electric power to the instruments failed on the liftoff of the

1981 Bubble Machine I, but useful optical data were obtained. The third flight a year later produced useful data from all but the electron detector on the ESA. Ground based optical and telluric field instrumentation recorded evidence for injection induced waves of about 5 second period. Delay times indicate a slow (175 - 385 km/sec) propagation from the burst point. Concerning locally produced electrostatic instabilities the wave measurements indicate that finite Larmor radius stabilization occurs for the weakly driven low (barium) density situation, but that shorter wavelength waves can occur early in the expansion event when the barium density is higher. These results are in reasonable agreement with a theory described by Sperling and Krall (1981).

I. Introduction

Taurus Tomahawk rockets containing high explosive shaped charges with barium liners were launched from Poker Flat, Alaska in March 1980, 1981, 1982. The shaped charges were designed to make waves by perturbing the ambient plasma and magnetic field by injecting a thin sheet of barium gas radially perpendicular to the B field. The 1981 and 1982 experiments were a mother-daughter combination, with the mother containing instrumentation for measuring fields and plasma parameters about a km away from the detonation. An electrical power failure at lift-off on Bubble Machine I eliminated the instrumented experiments, but the repeat experiment Bubble Machine II a year later worked well. Ground based data were obtained in all experiments.

The instrumented section of the Bubble Machine II rocket remained attached to the Tomahawk motor and consisted of a single axis (3 m tip to tip) dipole electric field detector operated from dc to VLF frequency, and a fixed bias cylindrical Langmuir probe supplied by Cornell University. A fixed energy (240 eV.) electron retarding potential analyzes, (RPA) and curved plate energetic ion and electron electrostatic analyzer (ESA) were supplied by the University of California at San Diego (UCSD). One of the ESA's was devoted to ions; the other to electrons. Both swept from about 50 eV/q to 10 keV/q with a spectrum obtained in approximately 125 m sec. Good data were obtained from all detectors except for the electron channel on the ESA. Space was quite limited and precluded inclusion of a full attitude determination system. A three axis magnetometer yielded aspect with respect to the magnetic field. It should be noted that a single axis dipole detector can only receive a single component of any electric field fluctuation which takes place more quickly than one half of the rocket spin period.

Launches were planned for quiet conditions so that the effects of the perturbation would be evident in situ and at remote sensors on the ground. A telluric current recorder located at Poker Flat measured the voltage across a 1.597 km long, magnetic N-S oriented grounded dipole. VLF emissions were also recorded from an antenna located on a ridge near Poker Flats. The injections occurred above 460 km altitude, and were observed with optical instrumentation from sites in Alaska and from the NASA Ames Learjet.

The shaped charge detonation did make waves. Various aspects of the experiments are discussed in the following sections.

II. Data Presentation

High Explosive Radial Shaped Charges: Neutral Gas Dynamics The high explosive shaped charges used in the Bubble Machine I and II were an improved version of the first King Crab device (Wescott et al, 1981). Figure 1 shows a schematic drawing of the device. 4.5 Kg of comp. B high explosive formed the shaped charge surrounding the 1.04 Kg V-shaped ring liner of barium metal. Detonation occurred at the center of the shaped charge. The pressure of the explosion on the barium liner causes it to collapse and partially vaporize. We have assumed 15% vaporization, but this number is not well known. Michel (1974) concludes that 27% vaporization is the theoretical limit in a 30° conical Ba shaped charged. Michel, (1969) measured 11% in a small laboratory shaped charge and estimated 20% for a full scale model. Some of the vapor is accelerated to high velocity radially with a small angular distribution about the plane perpendicular to the axis. Figure 2 shows the velocity distribution measured from TV signal intensity for Bubble Machine II. Initially, the barium gas has a small initial fraction of ions created in the explosion process. Estimates of the thermal ionization fraction range from $\eta \approx 10^{-3}$ to $< 10^{-4}$, Haerendel (1982). Further ionization is produced by by several processes. The releases are carried out in full solar u.v. radiation which produces ions with an exponential time constant of about 20 seconds Michel (1969). In the case of radial injection perpendicular to the field, the gas with velocity greater than 2.7 km/sec exceeds the Alfvén critical velocity for self ionization, and when the density is appropriate some ions should be produced by the Alfvén mechanism (Alfvén, 1954; and Arrhenius, 1975; Deehr et al., 1982; and Haerendel 1982).

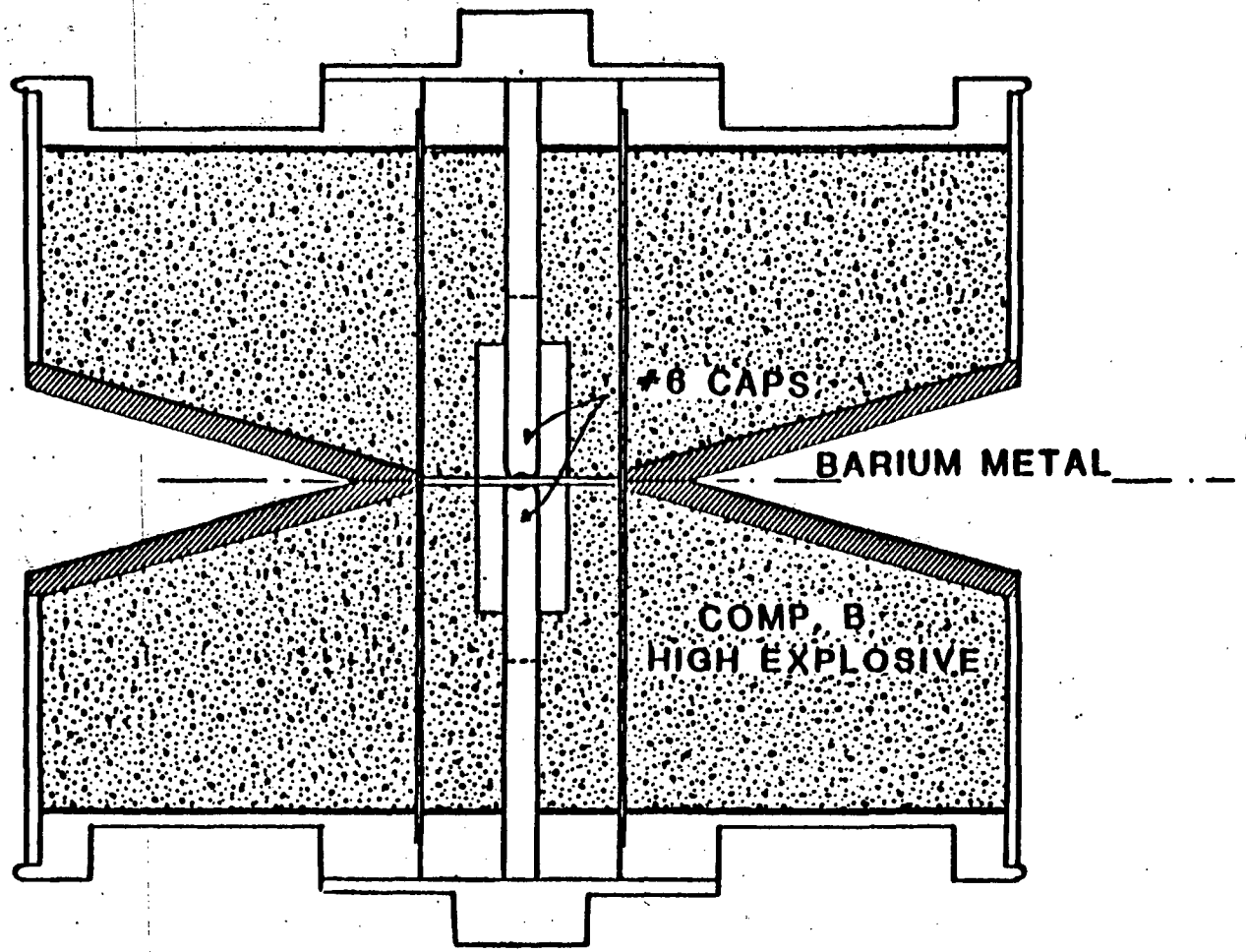

Figure 1. Cross section schematic drawing of radial high explosive shaped charge used in Buble Machine I and II. Detonation is at the center causing the liner to collapse and Ba gas to jet out horizontally with radial symmetry.

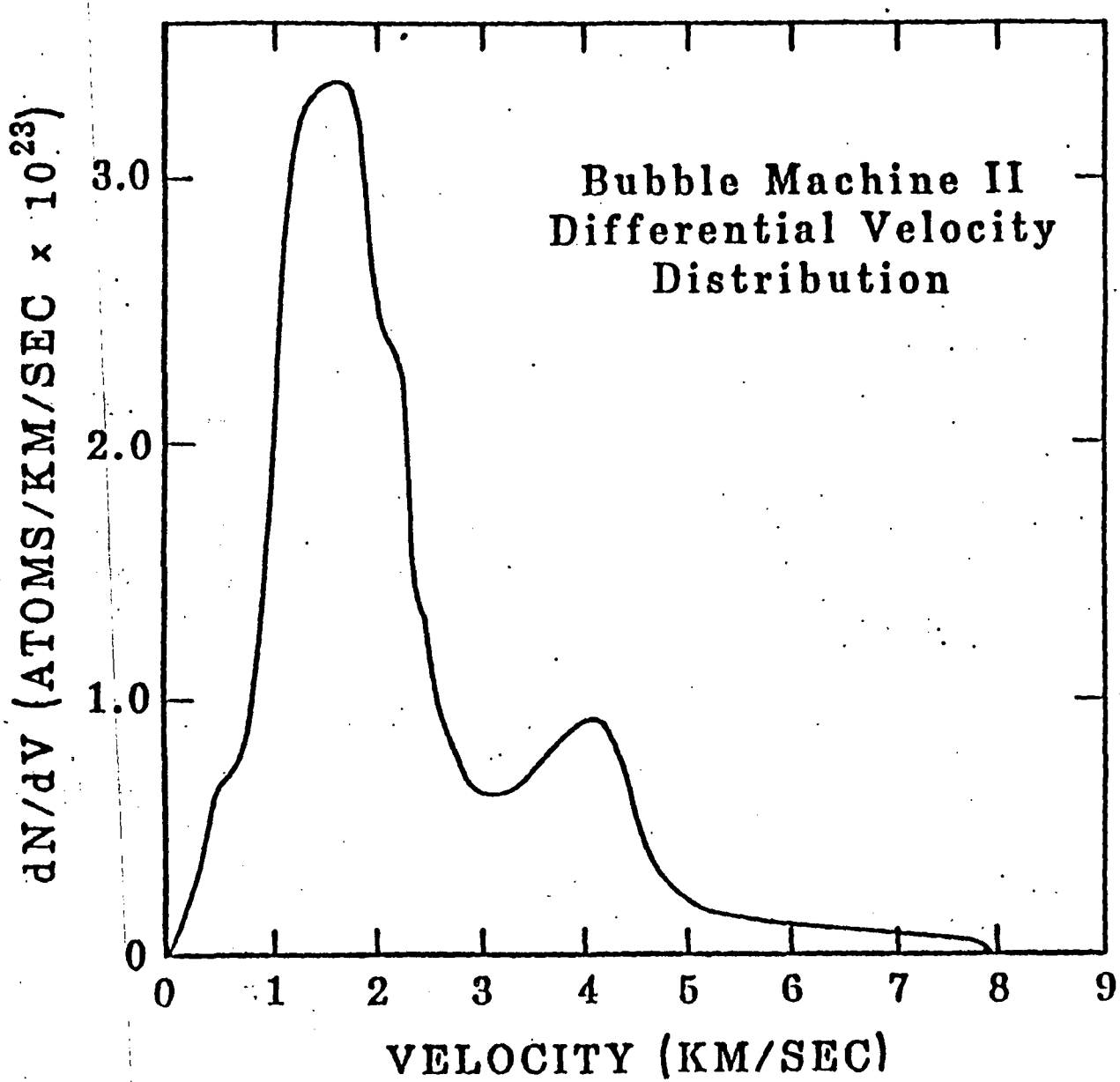

Figure 2. Differential Ba atom numbers vs radial velocity distribution, Bubble Machine II derived from TV signal level scans. Fifteen per cent vaporiztion of liner was assumed to assign number scale value.

There have been four radial shaped charge injection experiments (Wescott et al., 1980, Deehr et al., 1982 have described the first two). Although differences have been observed between them, we can describe the typical features. The barium metal liner is vaporized and comes out in a thin sheet radially. As soon as details can be detected in TV or film camera pictures (about 3 seconds after detonation) the neutral barium gas can be seen to have finger like wispy jets at the leading edge, and blob-like irregularities in the slower portions. The wispy jets have velocities ranging from 6-8 km/sec. The annulus of blob-like irregularities has material traveling from 3 to 4.5 km/second. The bulk of the gas has velocity from 0.94 to 2.6 km/sec and is in an inner annulus also with irregularities. Bubble Machine II was observed from a NASA Learjet flying over British Columbia. The view was almost from the side allowing calculations of the thickness of the torus of slow barium gas (Figure 3). When the slow ring had expanded to a diameter of 45 km, video signal scans across the major and minor axis provided a measure of a half angle of 13 degrees for the torus.

Barium Plasma Effects: King Crab Revisited

As the neutral gas expands outward any barium ions formed are held by the magnetic field lines and left behind. In the absence of an electric field as in the King Crab experiment, (Wescott et al., 1980) the ions appear in a stellate "wagon wheel" configuration. There is a central region depleted in ions which appears as a black hole. For reference Figure 4 shows the Ba ions left behind in the "King Crab" experiments. The diameter of the black hole was about 5 km.

The King crab experiment was the first radial shaped charge experiment, launched on a Taurus Tomahawk rocket 16 March, 1980 (Wescott et al., 1980). Detonation occurred at 1202:10UT at an altitude of 571 km. There was

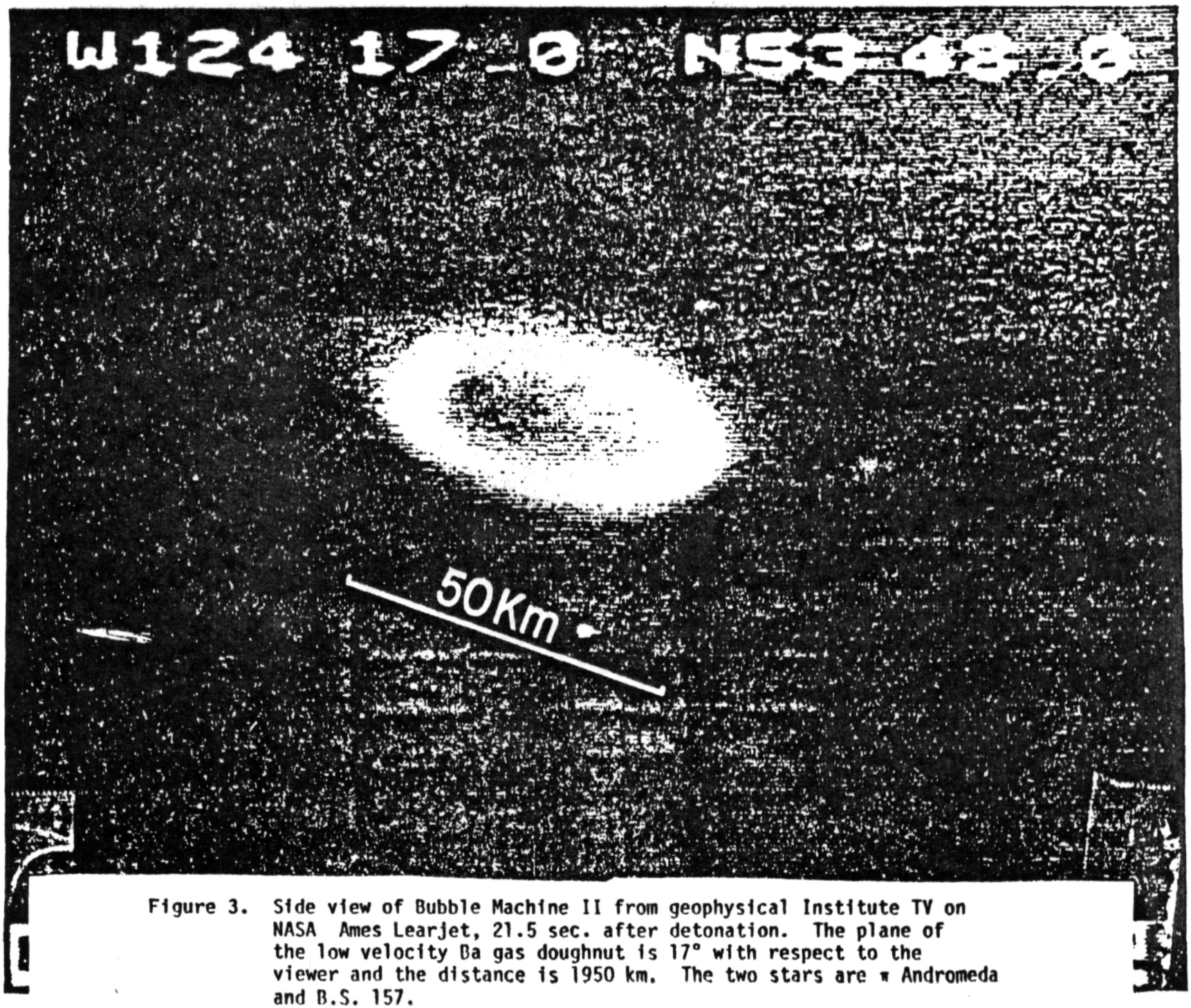

Figure 3. Side view of Bubble Machine II from geophysical Institute TV on NASA Ames Learjet, 21.5 sec. after detonation. The plane of the low velocity Ba gas doughnut is 17° with respect to the viewer and the distance is 1950 km. The two stars are ν Andromeda and B.S. 157.

almost no convection electric field as the stellate ion structure was observed for 11 minutes without drift motion and distortion. The Chatanika incoherent scatter radar also detected no electric field (J. Vickery, private communication, 1980). However background levels of VLF and ELF noise were evident at the burst time. The auroral background at 4278 A was also high and pulsating at the burst time. Therefore the natural background noise masked any detonation produced effects.

The black hole and ion rays are the most interesting feature of the King Crab experiment. There were about 18 bright rays emanating outwards from a 5 km diameter region depleted in ions. Figure 4 shows the TV view from Ft. Yukon, Alaska looking nearly in the magnetic zenith. From Ester Dome, about 25° away from the magnetic zenith, the black hole is elliptical with elongation in the magnetic field meridian. Understanding this feature was one of the goals of the Bubble Machine I and II experiments. Before presenting the new data, we first summarize our knowledge of the black hole formation based on the King Crab results.

The observed velocity distribution of the neutral Ba atoms (Figure 2) shows a pronounced peak at 1.6 km/sec of 3.4×10^{23} atoms/km/sec. At 1 km/sec. there are still 1.8×10^{23} atoms/km/sec. At these low velocities the ion gyro-radius is 49 and 31 m respectively for these two velocities, so any ion created by solar u.v. irradiation should gyrate closely around the field line where it began. If nothing acted to change the situation there should be a high concentration of Ba ions surrounding the burst point. Some efficient process must have acted to allow all or most of the barium ions to escape from a black hole of diameter about 5 km.

If the magnetic field were reduced to a low level, the ions as created could continue radially outward as the gyroradius is proportional to 1/B. For instance a 1.6 km/second ion in a 960 nT field has a gyroradius of 2.5 km.

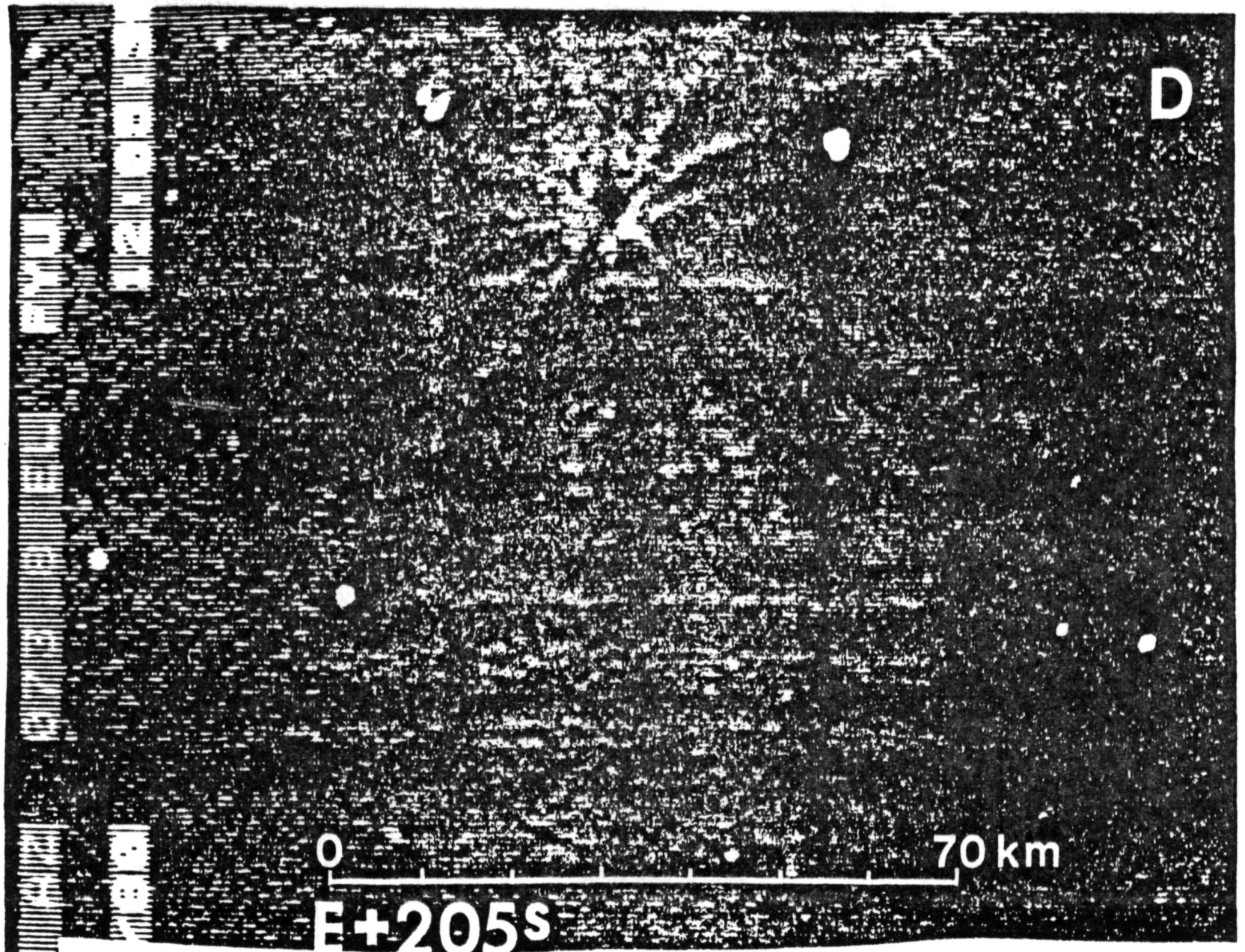

Figure 4. TV view of the stellate ion structure produced in the March 16, 1980 King Crab experiment 205 seconds after detonation. The inner hub region depleted of ionization is called a black hole. An almost complete absence of an ionospheric E field allowed the structure to be seen for about 20 minutes.

There is not enough kinetic energy in the neutral Ba gas to create a magnetic bubble that large. Assuming 15% vaporization of the liner, and the differential velocity distribution of Figure 2, the total kinetic energy is 540 kJ. If this energy was totally dissipated in annihilating the magnetic field, a spherical magnetic bubble of diameter 1012 m could be created. However, we know that the neutral Ba expanded outward from the burst point with no apparent retardation, so only a fraction of the kinetic energy was lost. In Figure 5 we have plotted the collision frequency between a magnetized Ba ion and the neutral Ba atoms streaming past it at time 100 m sec after burst and the differential energy distribution. There is much more energy in the peak near 4.2 km/sec than near 1-2 km/sec. but the collision frequency is much lower. Thus the more dense low velocity barium gas can couple energy from the neutral to the ions and magnetic field by collision processes while the high velocity gas cannot. The energy in the barium neutral gas travelling between 0 and 3 km/sec is 166 kJ, sufficient to create a magnetic bubble 680 m in diameter if the kinetic energy were totally expended. Obviously only a fraction of the energy of the neutral gas was transferred to the ions and magnetic field. Collisions are significant out to a few hundred meters given the assumption that only 15% of the barium was vaporized. We have no firm data to verify the vaporation efficiency. If a greater percentage of the barium is vaporized the effect of neutral-ion coupling would be effective out to a larger radius.

The gases produced by the 4.5 kg of high explosives may contribute to the snow plow effect sweeping out ions. The detonation of 4.5 kg of Comp B would produce 141 moles of gas products, primarily N_2, CO, CO_2, CH_3OH and lesser amounts of CH_2O_2, CH_4, NH_3 and H_2O. The gases at detonation have a temperature of 4420°K and an expansion velocity of 7.84 km/sec (Cook, 1971).

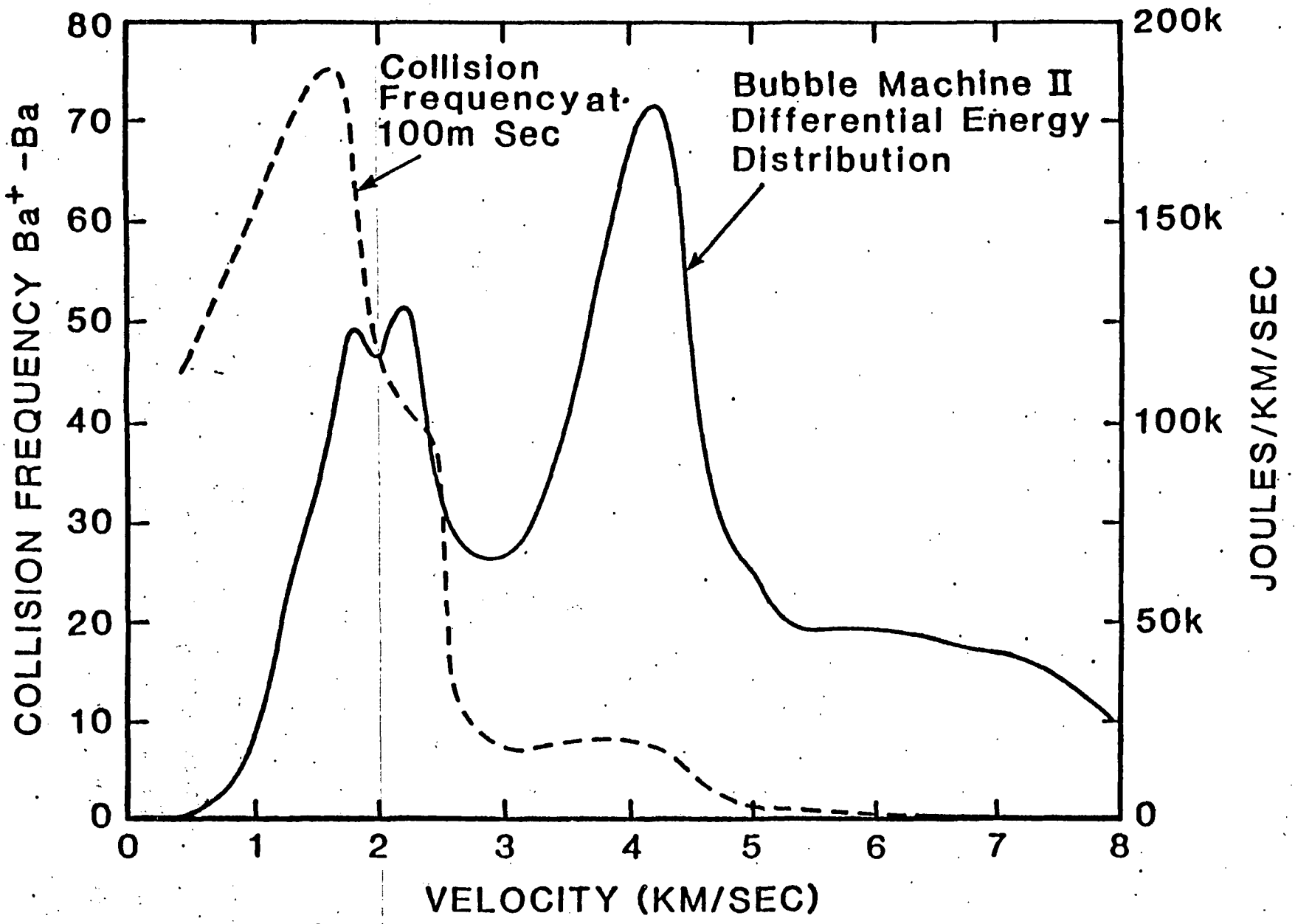

Figure 5. Plots of the differential kinetic energy vs velocity, Bubble Machine II experiment and the collision frequency between a barium ion and the streaming neutral barium gas at 100 msec after the burst. Note that although the highest energy is centered near 4 km/sec., collisions are too infrequent to couple energy from the neutral gas to the ions and magnetic field. Energy can be transferred near the low velocity peak near 1-2 km/sec.

If we assume all the gas is in a spherical shell from 7 to 8 km/second, then the collision frequency between an atmospheric ion, or a Ba ion and the explosion gas at time 100 m sec is 1243/sec, and falls off as t^{-3}. The actual density distribution is more likely to approach a Maxwellian distribution, and the collision frequency would be lower. Also the molecular weight of the gas products is much less than Ba so the momentum transfer from the light gas molecules to Ba ions will be less. The explosive gas products thus do not seem to be effective in sweeping out Ba ions for more than the order of 100 m radius, and the velocity exceeds most of the barium gas, so most of the ions would form behind the gas front.

We also investigated the possibility that the explosive gases might absorb solar UV, preventing ionization of the expanding Ba gas for a period of time approximately 2.5 seconds. However, none of the gases has a significant absorption cross section in the 3000 A region, and the number of molecules in the path length is at least four orders of magnitude below the amount necessary to produce significant UV absorption.

Similarly the argument that the barium gas is optically thick for about 2.5 seconds does not hold up to simple calculations. Also if the optical thickness were responsible for the black hole, the inner edge would not have a steep gradient as the barium thinned out. Yet the appearance of the hole is sharp (see Figure 4).

Barium Plasma Effects: Bubble Machine I

The payload consisted of the 4.5 kg radial shaped charge on a spring loaded separable daughter section and an instrumented section attached to the Tomahawk motor. All power to the instrumented section and the separation mechanism failed at lift off so only ground based optical and other observations are available. Detonation occurred at 08 10 55 UT 25 March 1981

and at 66.08° lat. 146.47°W long., 495.7 km altitude. Kp was 5- during the three hour interval of the experiment, but it was quiet magnetically at College during the event. As evidenced by the rapid convection of the Ba^+ ions there was a substantial DC electric field. The event occurred well polewards of diffuse bands of aurora. The aurora was quiet and homogeneous over the northern half of the sky. Meridian scanning photometer records in 6300 A, 5577 A and 4278 A indicate a characteristic energy deposition of approximately 600 eV to 1 KeV with a number flux of approximately 10^8 electrons/cm^2sec. The 4278 A emission was about 200 Rayleighs.

Two photometers at Ester Dome, Alaska, with narrow bandwidth filters at 4278 A were aimed near but below the burst point, and in the E region magnetically conjugate to the burst point to look for induced auroral emissions. Figure 6 shows the traces of the two 4278 A photometers during the event. A damped oscillation of about 5 second period is clear from both records but there is a delay of about 1 second at the 100 km level. The 500 km photometer was moved 3° in azimuth between 5 and 8 seconds after the event which had very little effect because of the high elevation angle. It was moved in elevation towards the neutral Ba cloud at 14 seconds, so the two traces are not expected to correlate after that time. The amplitude of the oscillation in 4278 A was somewhat larger in the 100 km trace. The auroral perturbation at both elevations begins with a decrease in the 4278 A background emission, and the modulation is about 50%. The period of the oscillation increases with time: the first cycle is about a 4 second period, the second 5 seconds, the third about 6 seconds.

Barium Plasma Effects: Bubble Machine II Bubble machine II was launched on March 15, 1982 with detonation at 06:43: 59.233 UT and at 66.13°N lat., 146.325°W long. and 460.11 km altitude. The injection was viewed by use

Figure 6. Comparison of 5° field of view photometers with 4278A interference filters looking near the Bubble Machine I burst region (upper trace) and in the 110 km region near the foot of the burst point field line. Note the one second phase shift between the upper and lower traces. A damped oscillation in the 4278A emission with about a 5 second periodicity commences with a decrease.

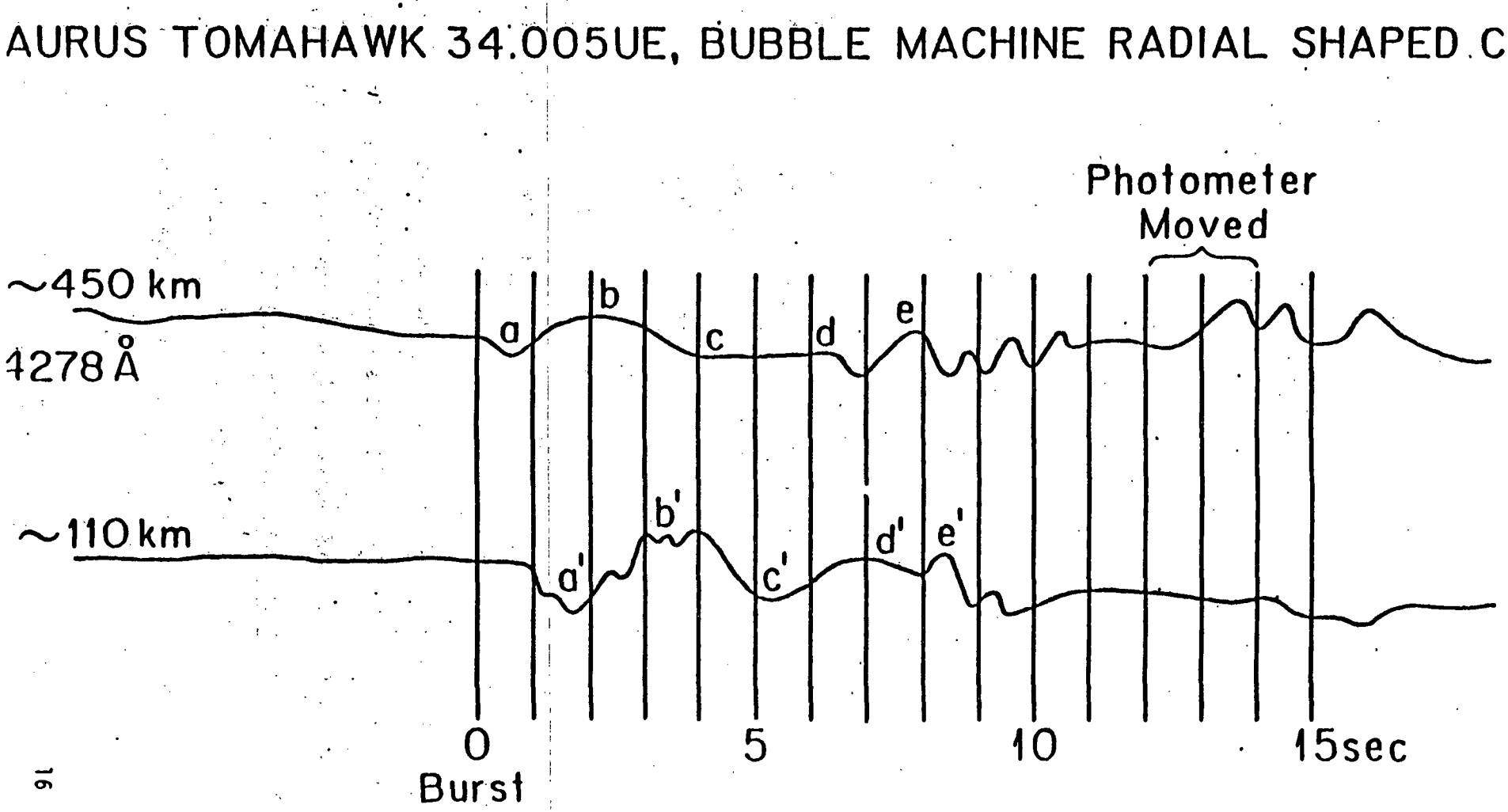

of image orthicon TV systems at Ester Dome (64.88° N, 148.05° W) and Fort Yukon, Alaska (66.56° N, 145.22° W) and from the NASA Ames Learjet flying over Prince George, British Columbia (53.81° N, 124.29° W). The Learjet was positioned to provide as near as possible a side view of the injection. Figure 3 shows a view of the slow material (1-2 km/sec.) from the Learjet. The slow barium appears to have the form of an expanding doughnut. Figure 7 shows a view of the neutral Ba gas at 5 seconds after detonation from Ft. Yukon looking almost perpendicular to the plane of the injection. The half angle of the doughnut out of the plane of injection measures 13°. This applies only to the slowest Ba gas as the TV was overdriven at earlier times when the fast jet material could have been seen. For calculations of Ba density and collision frequency we have assumed 13° for all the material.

Although the magnetic activity at the time of detonation was quiet, a substantial E field existed in the detonation region. Although the classic King Crab black hole and stellate Ba ion structure was probably formed, the $\vec{E} \times \vec{B}$ drift rapidly distorted and blurred the structures. The observed average ion drift velocity was 1.06 km per second, implying average E fields: E_N = 38.9 mV/m and E_E = 2.8 mV/m.

The main rocket payload with its instrumentation could be observed on film and TV pictures. Triangulation and least mean square fitting to a trajectory has produced an estimate that at burst the mother was 0.384 km south, 0.505 west and 1.065 km below the burst point for a total separation of 1.24 km. The magnetic field line threading through the instrumented payload was 824 m radially from the burst point in the plane of the injection. The triangulated toroid dips about 2° to the northwest.

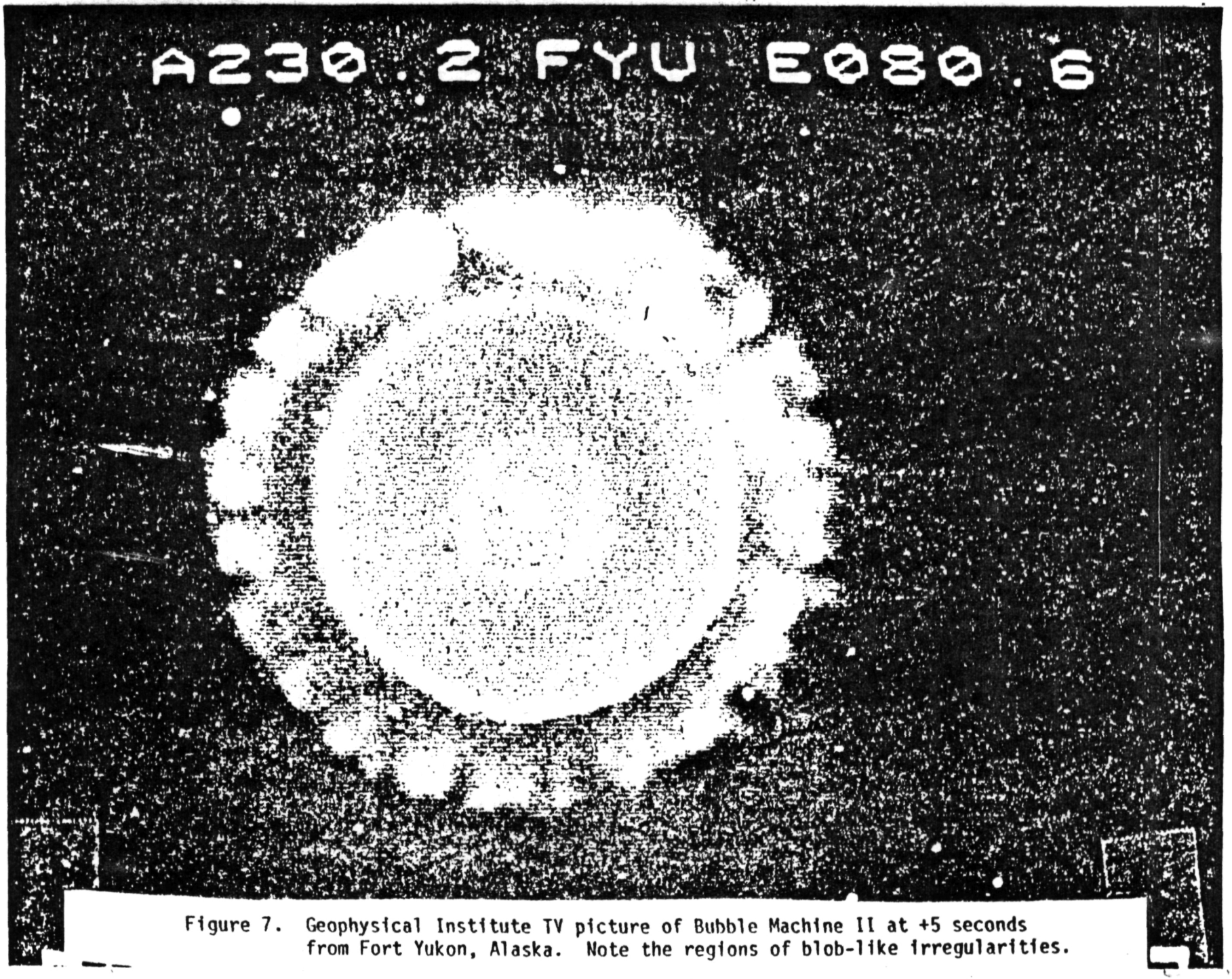

Figure 7. Geophysical Institute TV picture of Bubble Machine II at +5 seconds from Fort Yukon, Alaska. Note the regions of blob-like irregularities.

If we assume that the barium ions were pushed out of an area within a 2.5 km radius as observed in the King Crab experiment (Wescott et al., 1980) in a period of 2.5 seconds as implied from the slowest material, then we can build up a scenario as shown in Figure 8. The figure shows the location of the ring of ions surrounding the black hole at +1, +2 and +3 seconds under the influence of the background E field and the neutral collisions. The neutrals and ions would have originally passed over the instrumented rocket in about 300 msec while the ionization process was in progress. Then for about 2 seconds the instrumented rocket should have been within the Ba ion depleted region. At about +2.5 seconds the $\vec{E} \times \vec{B}$ drift would have brought the concentrated ion ring back over the instrument.

The telluric E field at Poker Flat was measured using a 1.59 km grounded dipole oriented nearly magnetic N-S (at N 25°E). The data storage system was capable of recording 190 seconds of data taken at 3 samples per second. Figure 9 shows the telluric E field data which contains the time of the Bubble Machine II detonation. The data in Figure 9 have been smoothed using a three point running average. The time of detonation is denoted as t=0 on the data plot and occurs approximately 20 seconds into the data record.

Two features stand above the background noise in the telluric data. the first is a two-cycle wavelet commencing about 2 seconds after the burst and the second, similar wavelet of smaller amplitude occurs approximately 140 seconds after detonation. Both of these pulses have periods of approximately 5.5 seconds. A somewhat longer period variation occurs near the 100 second mark. The peak to peak amplitude of these pulses in the first wavelet is about 10 mV/km. These are the only pulses of this type observed during a few hours data collection both before and after the experiment.

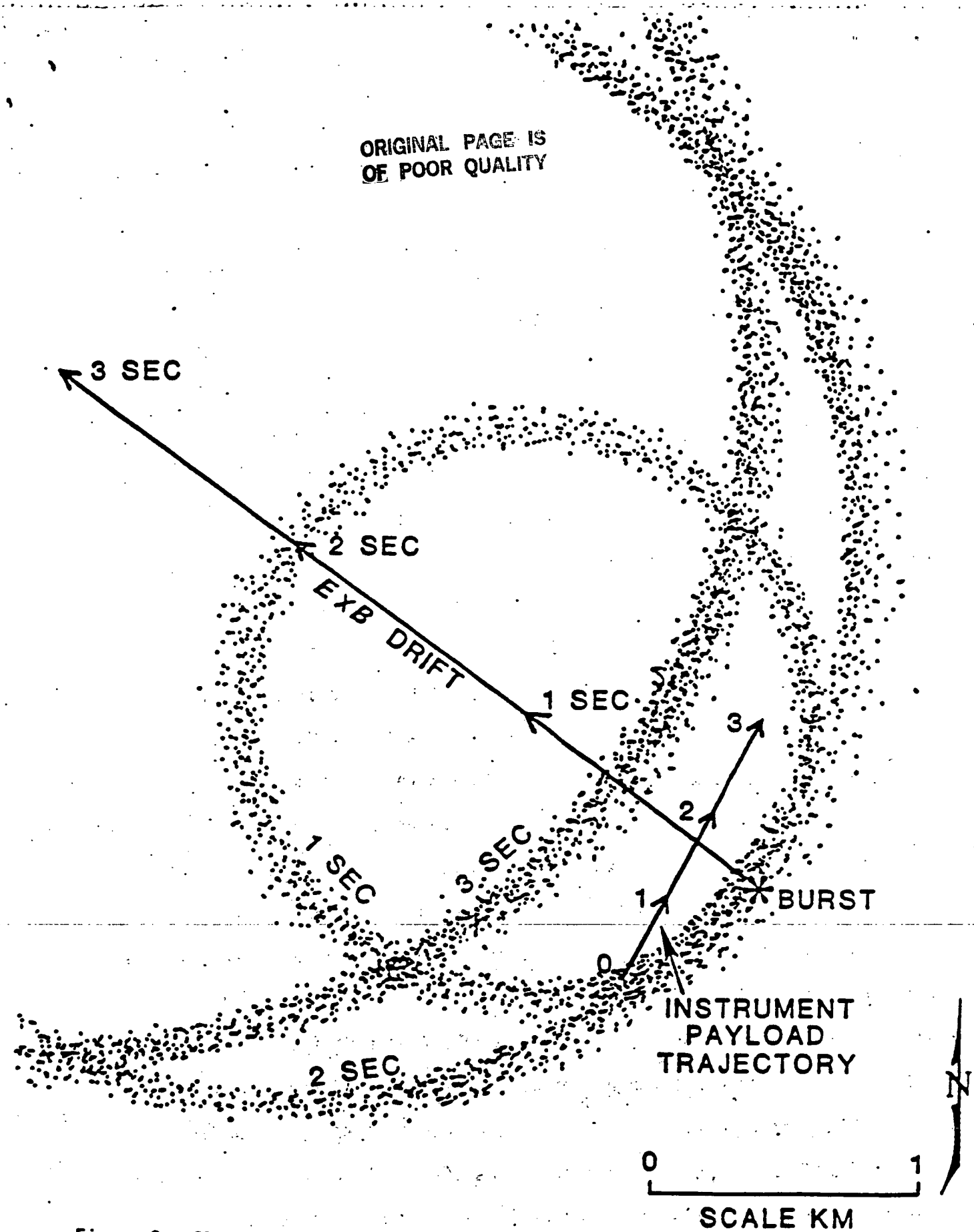

Figure 8. Plan view of part of the ion ring surrounding the black hole of Bubble Machine II at one second intervals. The position is due to the forces acting to push the ions outwards to about 2.5 km and the EXB drift to the northwest. As a result the ions would sweep across the instrumented payload for about 300 ms then return starting about 2.5 seconds after burst.

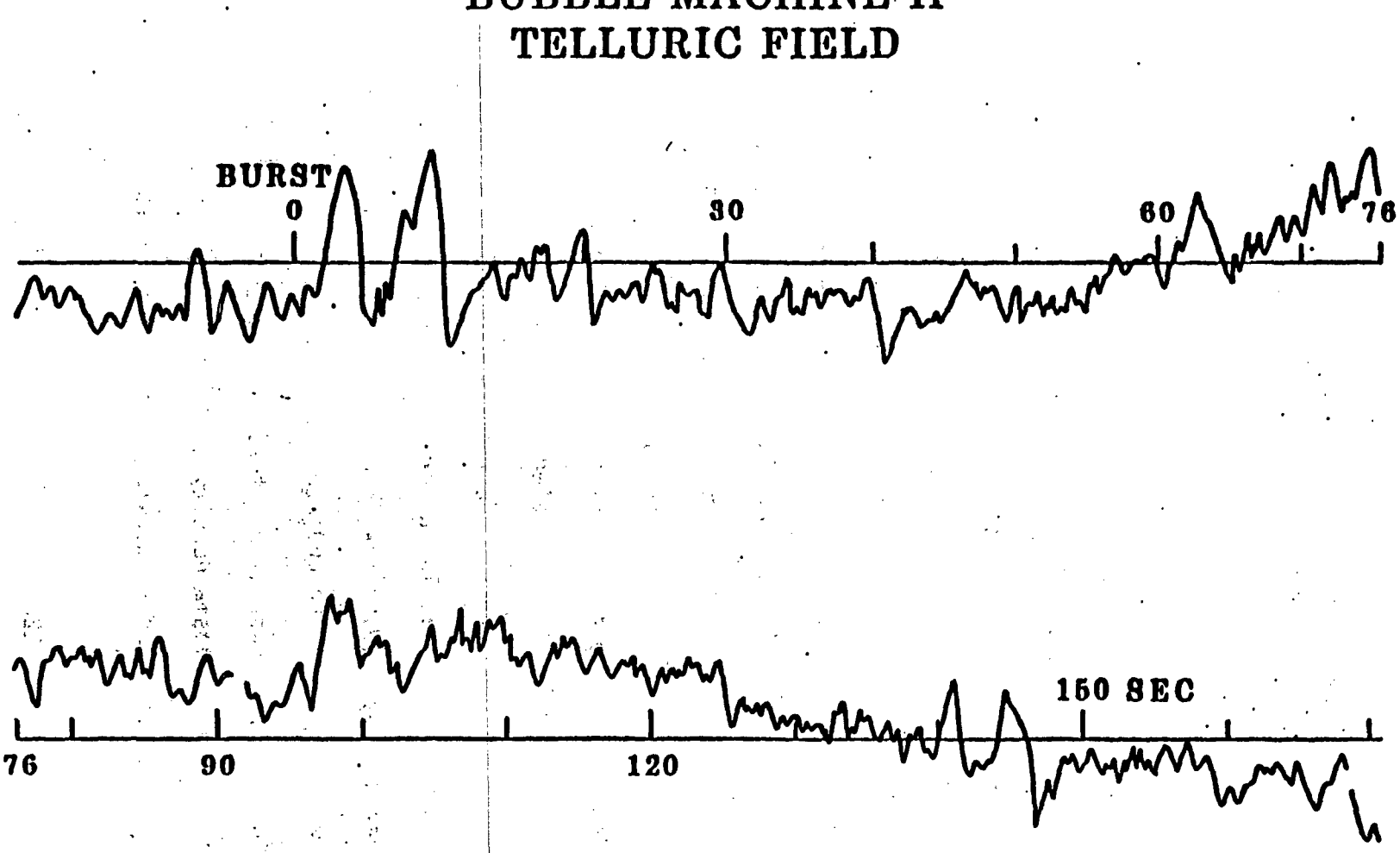

Figure 9. Recording of the voltage across a 1.6 km grounded dipole oriented close to magnetic north south at Poker Flat, Alaska, during the Bubble Machine II event. The two cycle pulsation commencing two sec. after burst appears to be a result of the explosive Ba perturbation The two cycle wave commencing at 140 sec. is consistent with Alfvén wave propagation to the southern conjugate ionosphere and return.

The telluric system had been used in other experiments to measure the effect of auroral magnetic disturbances on telluric electric potentials. During these previous experiments a system response in the frequency range of interest was established such that E = k dB/dt. For E in volt/km dB/dt in nT/sec, k = 0.1. (dB/dt is measured for the horizontal magnetic component perpendicular to the line.) The measured system response of 10 mV/km would imply a wave in the east west component of the magnetic field of about 0.1 nT amplitude.

Corresponding pulses could not be found in the magnetometer records from the rocket payload which had threshold sensitivity of 50 nT. Pulses were also absent in the induction coil magnetometer on the ground at College, Alaska. The induction coil had a threshold noise level of 4×10^{-4} nT in the 5 second period band. If the pulses are assumed to be electromagnetic wave estimates of the E/B ratio indicates the magnetic component ground amplitude would be approximately 1/10 the noise level and undetectable.

We turn now to the results of the instrumented portion of the Bubble Machine II payload. A frequency-time-intensity (sonogram) plot of the VLF waves (10-16,000 Hz) detected during a time period centered on the burst is presented in Fig. 10. The data are from the electric field instrument. Natural VLF emissions were detected after the burst with frequency and temporal characteristics typical of similar auroral experiments (Temerin and Kelley, 1980). They display a sharp low frequency cut-off at the lower hybrid frequency. If we assume that the undisturbed plasma is entirely composed of O^+ ions, the observed lower hybrid frequency at a flight time of 360 seconds implies an ambient plasma density of $5 \pm .4 \times 10^4$ cm^{-3}. There is no reason to suspect that these emissions were caused by the explosion.

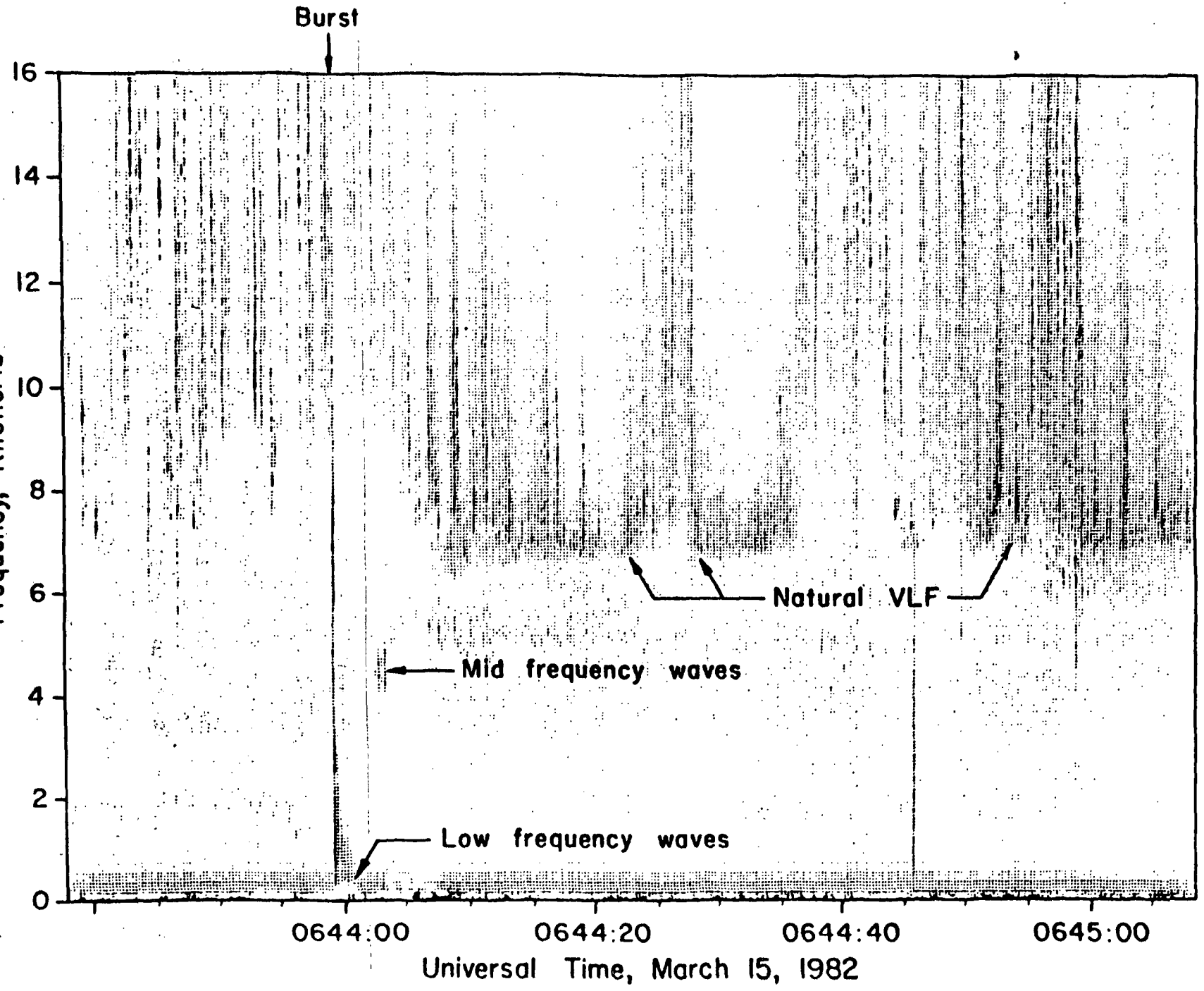

Figure 10. A VLF sonogram showing electric field fluctuations intensity as a function of time and frequency.

The dark line at the burst time shows that intense broadband emissions accompanied the explosion, with the signal exceeding the instrument noise level up to at least 12,000 Hz. Low frequency emisions ($\leq$ 120 Hz) are also evident in the sonogram for several seconds (see discussion below) and an isolated burst of mid-band signal centered at 4.3 kHz started about two seconds after the burst. Directly after the burst the VLF signal seems to be suppressed for about one second at frequencies above the ambient lower hybrid frequency.

The low frequency waves were also detected by a fixed bias Langmuir probe showing their electrostatic nature. A sonogram of the low frequency (10-500 Hz) signal is presented in the top panel of Fig. 11. The burst time is indicated and again the intense initial broad band noise pulse is apparent. This is followed by a one second burst of signal at frequencies below 200 Hz. A gap in the emission strength then occurred for about two seconds which was followed by an extended period (~8 seconds) of emissions again well below 200 Hz. In fact, these waves display an extremely sharp high frequency cutoff just above 100 Hz.

The second panel shows a signal proportional to $\log_{10}$ of the current to a cylindrical fixed bias Langmuir probe. Care must be taken in interpreting this output due to possible vehicle potential variations in the chemically active environment. We monitored the potential difference between the skin and one of the spheres. In fact, during the initial post burst one second interval this channel displayed a total peak to peak variation of about 0.4V with a waveform similar to the relative density waveform plotted in Fig. 11. We determined the value of dI/dV for the Langmuir probe during much of the flight (LaBelle et al., 1982) and hence can estimate the apparent density

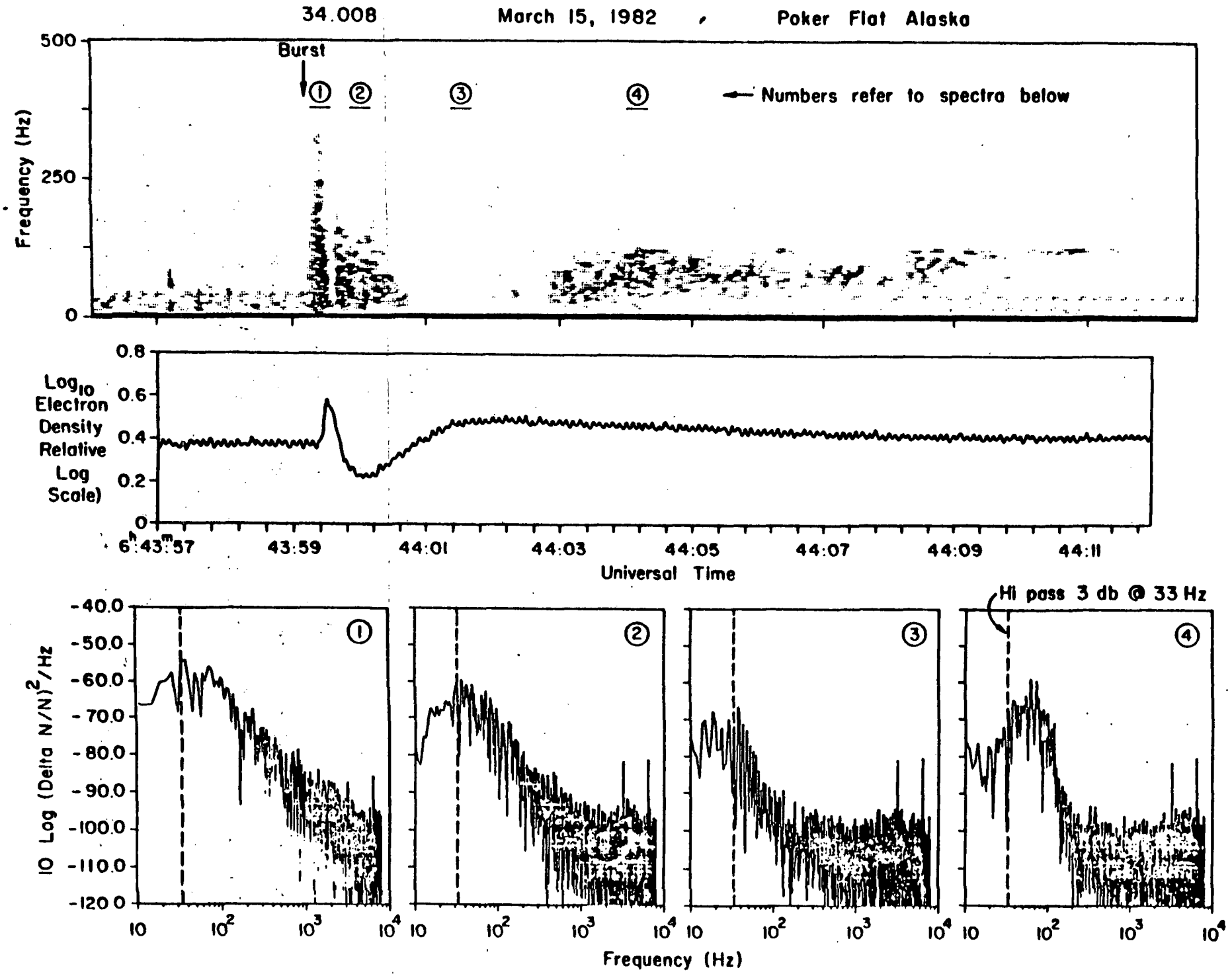

Figure 11. A low frequency sonogram showing the low frequency waves and representative power spectrum.

change under the assumption that the observed signal is entirely due to the skin voltage change (which is the Langmuir probe reference potential). About one-half of the total response observed can be easily explained in this manner and we conclude that the initial variations are not real density changes. However, by 0644:01 the vehicle potential returned to its pre-explosion level and remained there for an extended period. We thus conclude that at 0644:02 the payload was immersed in a plasma which was 25% more dense than the ambient plasma prior to the event. By 0644:11 the measured plasma density returned to the pre-explosion value.

The second burst of low frequency waves is well correlated with the density enhancement. They do not seem to be associated with the peak in the enhanced plasma density, but rather arrive on the "trailing edge" of the plasma. A similar relationship between emissions and plasma gradients has been observed in other chemical release experiments (Kintner et al., 1980; Kintner and Kelley, 1982). Notice that the waves near 4 kHz also occurred at a time when the plasma density was decreasing.

Representative $(\delta n/n)^2$ spectra are plotted in the bottom panel of Fig. 11 with labels corresponding to the time periods similarly numbered in the upper panel. The burst spectrum (#1) displays a $(1/f)^2$ form. Fixed bias Langmuir probes are sensitive to electric field variations under some circumstances (Kelley et al., 1982). However, comparison with the δE spectrum shows that the $\delta n/n$ variations are 15 db higher than those expected from coupling to the electric field. We thus conclude that electrostatic waves or a combination of electrostatic and electromagnetic waves are responsible for the burst waves. Similar conditions were met in considering burst related emissions in other experiments of this type.

Spectrum 3 shows how quiet the region of peak plasma density was. For example, at 100 Hz the signal is at least 30 db lower in spectrum 3 than in any of the others plotted.

Spectrum 4 shows the extremely sharp nature of high frequency cut-off in the signal. The steep signal decay begins at 120 Hz and falls off roughly as f^{-12} for f>120 Hz. Spectrum 2 also shows a high frequency cut-off above 10 Hz, but one which is much more gradual.

The integrated fluctuation strength in the band 70 - 120 Hz is plotted in Fig. 12 for the ($\delta n/n$) and (δE) receivers. The signal to noise ratio was better in the former detector due to the interference bands in the electric field channel which can be seen at low frequencies in Fig. 10. The modulations in the signal are mirrored in the two channels and are not related in any obvious way to the spin rate.

We are turning now to the dc electric field signature of the event. Previous explosive chemical release events have generated significant quasi-dc electric field probes. For example, the cesium lined spherical high explosive used in the Trigger experiment created a 200 mV/m electric field pulse (Holmgren et al., 1980). That pulse was followed several hundred ms later by an intensive field aligned electron precipitation event, consistent with instability of an upward propagating Alfvén wave (Kelley et al., 1980). In the present experiment, a quasi-dc electric field pulse was also observed but which lasted less than 100 ms and which had an amplitude of about 10 mV/m. A single dipole antenna can only measure one component of such a pulse and hence the measured value represents a lower limit on the field strength. Nonetheless, it seems clear that the radial shaped charge was less efficient in generating an Alfvén wave than the lower velocity (but higher plasma

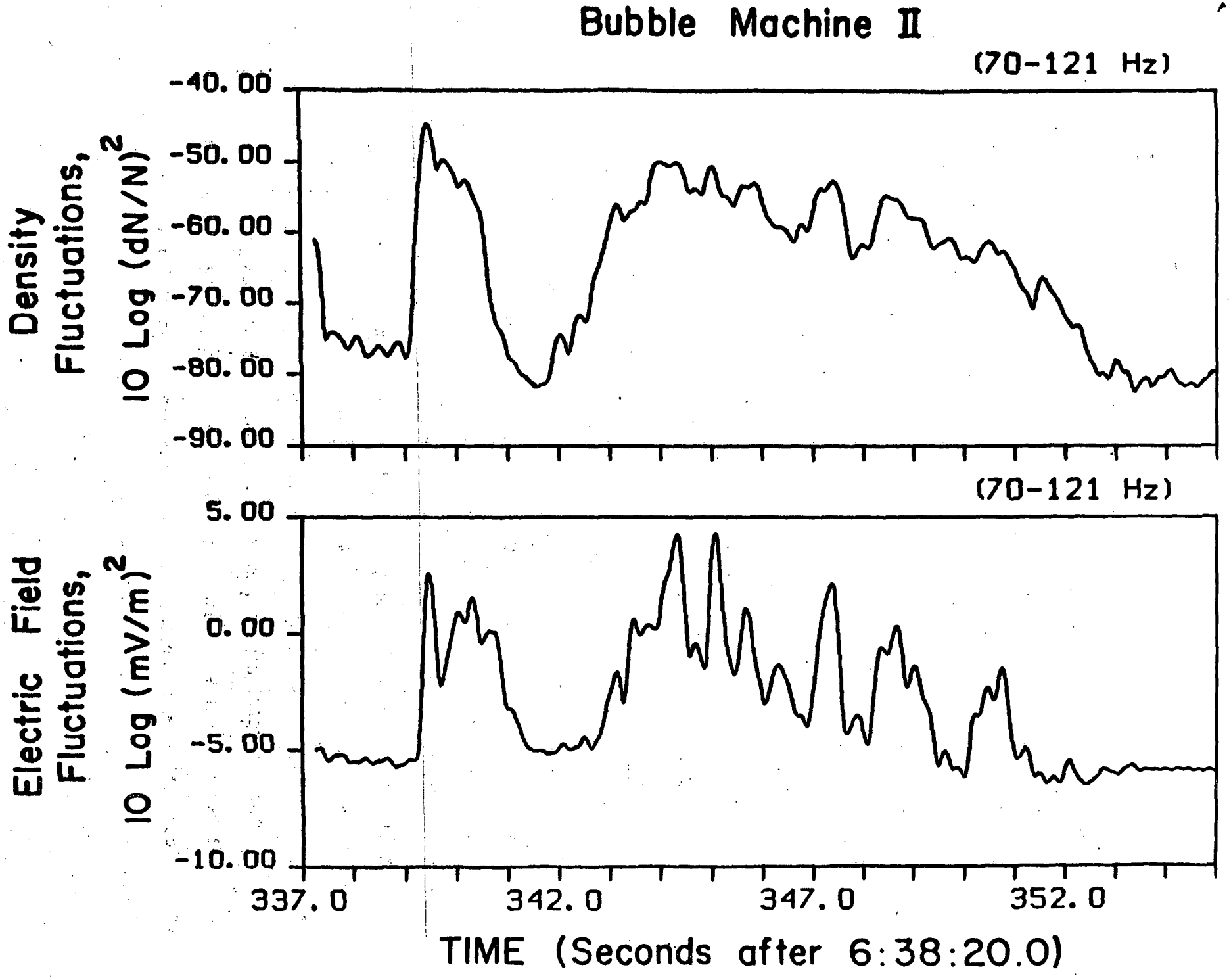

Figure 12. Integrated electric field and density fluctuation signal strengths versus time.

density) cesium experiment. The magnetic field measurement on board the rocket was sensitive to perturbations greater than about 50 nT. For an Alfvén speed of 500 km/s this corresponds to a 25 mV/m electric field perturbation. Thus, the absence of an observable magnetic field signal is consistent with the small electric field pulse. (In the most recent more efficient radial shaped charge experiment conducted in April, 1984 a much larger electric field perturbation was observed.)

Figure 13 shows the ion energy that was analyzed and the corresponding ion differential energy flux as a function of time during nearly one second around the burst time.

The ion ESA sweeps from 55eV to 10 keV in 125 msec, taking 12 steps of 4 accumulation times each. The downsweep followed the same pattern, with the energy levels staggered to lay between the upsweep levels. The pitch angle was within 10 degrees of the field.

We group these data into three periods of energetic precipitation: one centered at 6:43:59.33 UT, one long burst lasting between 6:43:59.40 and 59.54, and one final interval at 59.60. The energies observed ranged from the lowest level (nominally 55eV) to 6.8 keV (the highest energy level that the sweep included was 10 keV). Since the highest energy particles produced in the explosion are ~60 eV, kev energy particles must be assumed to be already present. The weak electric field (~10 mV/m) observed makes it unlikely that a large electrostatic shock could be responsible for accelerating the particles as was believed to be the case for Project Trigger (Holmgren, 1980).

Although the time resoltuion is not sufficient for a detailed dispersion analysis, it is worth noting that the observations do not fit a classic dispersion pattern of arrival from a distant source. Indeed the first

particles that are observed at 59.33 are of comparatively lower energy. This makes it likely that the source of the particles was close to the payload. It may be that the ions were already in existence and were simply scattered by ordinary ion-Barium neutral collisions into pitch angles near zero. This explanation would require that the distribution be sharply peaked at large pitch angles, since otherwise our detector (which was nominally aligned with the magnetic field) would have observed the energetic ions prior to the release.

Each period of ion precipitation can then be correlated with the passage of each of the neutral rings (shown in Figure 8) through the field line connected with the instrumental payload.

The Ba expands radially in an injection plane nearly perpendicular to the magnetic field. The time of arrival of the first ring at the field line connecting with the payload is 100 msec after the explosion; the first energetic ions are observed at 93 ± 18 msec after the explosion. This agreement is excellent, although the transit time for a O+ ion of the appropirate energy adds another 10 msec or so to the 100 msec figure. It is worth noting that the first ions are observed prior to the direct time of flight of the fastest debris from the explosion to the detector.

The second group of ions is first detected 172 ± 18 msec after the explosion. this corresponds very well to the time of arrival of the faster atoms in the second Ba ring to the field line connecting with the payload. Such atoms are moving at ~4.4 km/sec (refer to figure 2).

From figure 2 alone one might expect that the precipitation of ions would be continuous (perhaps with intensity variations) until after the passage of the slowest ring (peaked at 2 km/sec). Ions are indeed observed until the sweep returns to lower energy levels (this is why we include the

entire time 6:43:59.405 to 59.546 as one burst). The end of this burst at 59.546 corresponds to at transit velocity of 2.5 km/sec; there is no particular matching feature on the velocity distribution chart. We speculate that this simply represents a depletion of available energetic ions to be scattered; the passage of the previous Ba atoms could have by then essentially removed most of the energetic ions.

The final major observation of energetic ions occurs at about 59.625; this coincides both with the arrival time of the 2 km/sec peak and with the detector reaching the lowest energy resolution level (nominally 55 ev). Of the two possible factors, the latter is likely the most important. This is the only time near the explosion that the 55 ev level is measured. It is possible that there are far more comparatively low energy ions available to be scattered that there are in the hundred ev range or higher. Indeed, the explosion itself energized Ba atoms up to about 65 ev; some of these may have become ionized or transferred energy to thermal plasma ions.

Figure 5 shows the estimated collision frequency of ions with the neutral particles in the released cloud; it is high enough (on the order of 70/sec) that the scattering mechanism suggested here is plausible. Barium (atomic weight 137) is of course much heavier than the background plasma of mostly atomic ozygen and hydrogen, hence large angle scattering is more likely than would otherwise be the case.

The retarding potential analyzer, which was devoted to 240 eV electrons, recorded a single burst about 33 msec after the first ions arrived, and lasting approximately 10 msec. These data are shown in Figure 14 along with the pitch angle of the analyzed particles. It is not clear why there is only this single electron event. The fixed energy was chosen to be at

the peak of the electron spectrum seen in the Trigger experiments (Lundin, 1980). Thus, the absence of extended precipitation in these experiments contrasts greatly with those of Trigger. Both the particle data and the dc-electric results of Bubble Machine II imply a much weaker effect than in that experiment.

In summary, we have interpreted the particle results in terms of an already existing population of energetic ions pitch angle scattered by the released barium into the observation cone of the detector. This distribution must have been exclusively at large pitch angles in order to have avoided earlier detection by the ESA. Such a population is called an ion conic, and have been observed previously, although at higher atltitudes or lower energies in both (Gerney et al., 1981) and sounding rockets.

Yau et al. (1983) observed transversely accelerated ions (TAI) with pitch angles 90 to 130 in two sounding rocket flights into an active portion of the auroral zones at altitudes 400-600 km. These were in the range up to several hundred eV. The strongest TAI events tended to occur near regions of minimum energetic electron flux.

Thus, at least in the case of Bubble Machine II, there is little evidence that the energetic ions were created by the burst.

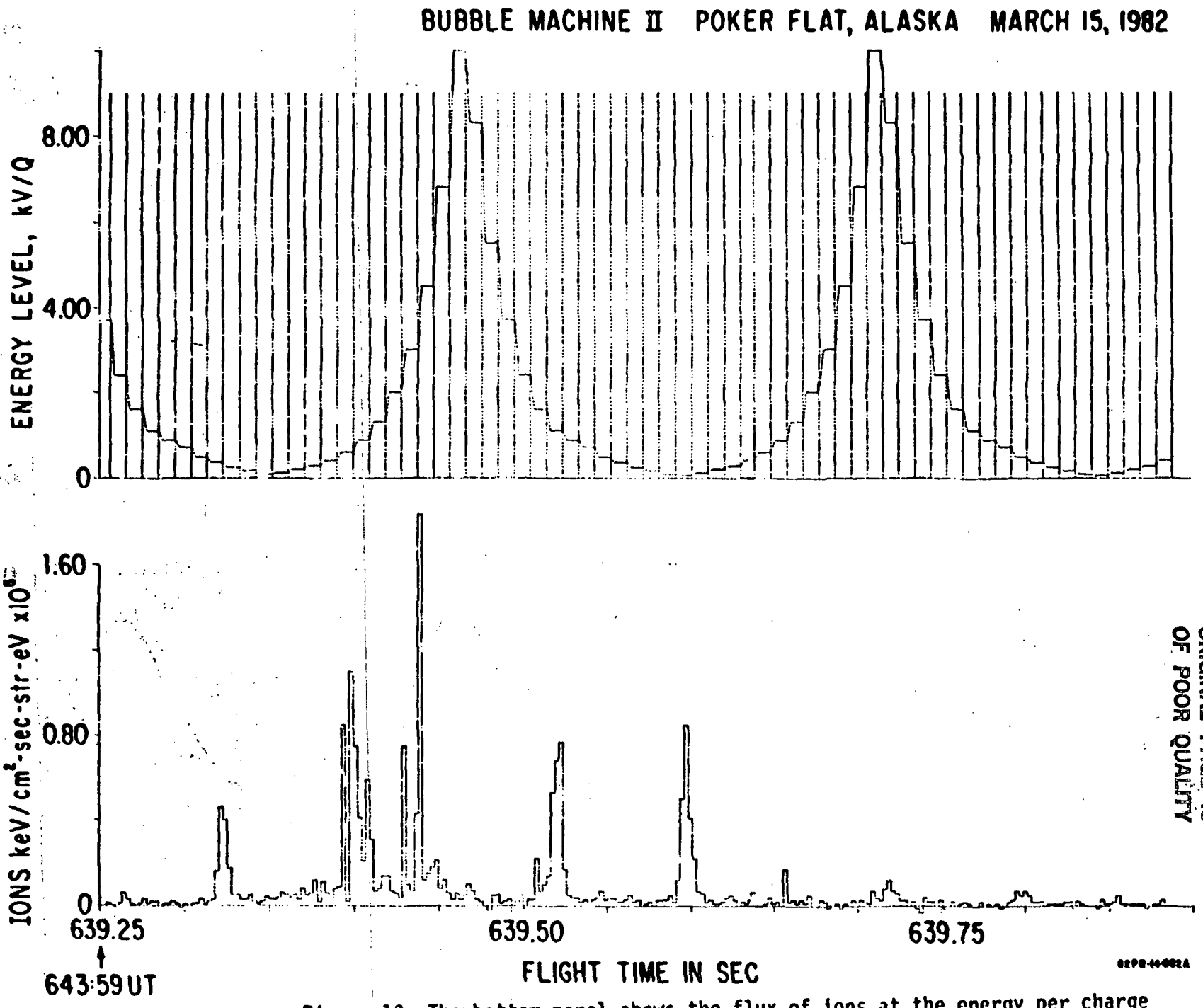

Figure 13. The bottom panel shows the flux of ions at the energy per charge shown in the bottom panel for about one second after the chemical ignition. All of these ions are at nearly 0 degree pitch angle.

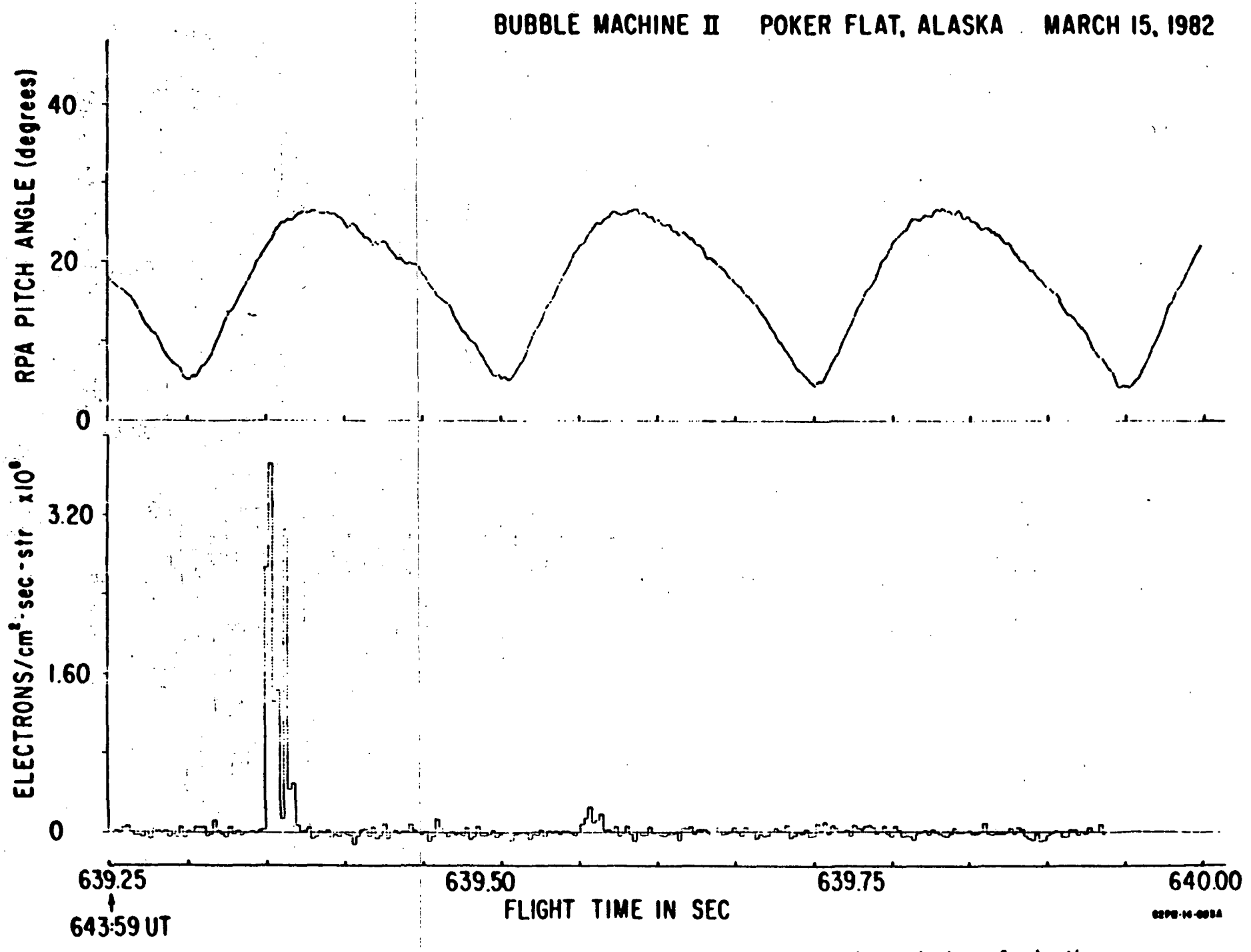

Figure 14. The flux of electrons at 240 ev at the given pitch angle in the top panel.

III. Discussion

A. Stimulated and Auroral Pulsations and Earth Current Modulations

The normal auroral luminosity vs height distribution has a maximum in the E layer. The altitude of the maximum depends upon the energy of the precipitating auroral electrons and the density of the upper atmosphere. The 4278A emission comes from the N_2^+ first negative band. If the atmosphere above 400 km is sunlit, resonance scattering from N_2^+ ions increases the volume emission rate so that the observed 4278A emission from above the sunlight line becomes significant with respect to the E layer peak. Figure 15 shows the estimated 4278A volume emission rate height profiles for Bubble Machine I. It is clear that there was sufficient 4278A emission near the burst where the photometer was pointed to allow the 50% modulation observed. Similarly at the lower photometer there is sufficient light to support a modulation. Deehr and Romick (1977) have reported a similar modulation of auroral emission due to a Ba thermal release near the same altitude. The question is how did the plasma perturbation physically induce the modulation in the light?

Figure 16 shows the fields of view of the two photometers with respect to the detonation, the 30 km screening height, the geometrical umbra and the aurora. It is conceivable that the two correlated auroral modulations are a coincidental natural pulsation in the main auroral luminosity near 110 km, but the auroral wave would have to travel polewards at 210 km/second horizontally. Cresswell (1968) has reported fast auroral waves in pulsating aurora with velocities ranging between 30 and 150 km/sec. The all sky TV located at Poker Flat does not show any detectable wave train, but the system is not very sensitive. It seems more likely that an oscillating perturbation began near the burst point and propagated down the field line in the E-layer. This implies a propagation velocity of 380 km/sec.

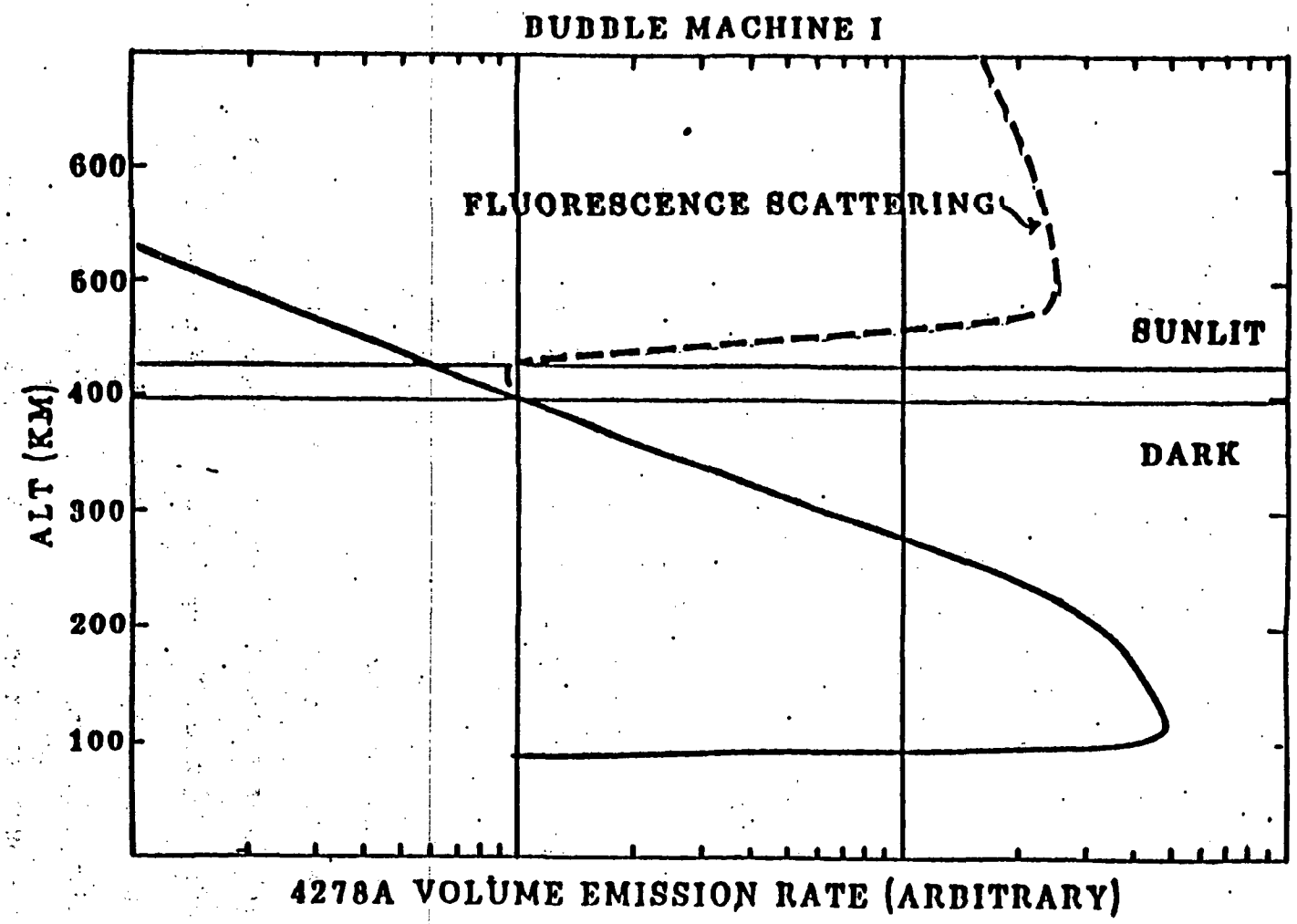

Figure 15. Volume emission rate of 4278A vs altitude, Bubble Machine I. Solid line is the normal contribution of the precipitating electrons. The dashed curve is the fluorescence scattering in the sunlit position.

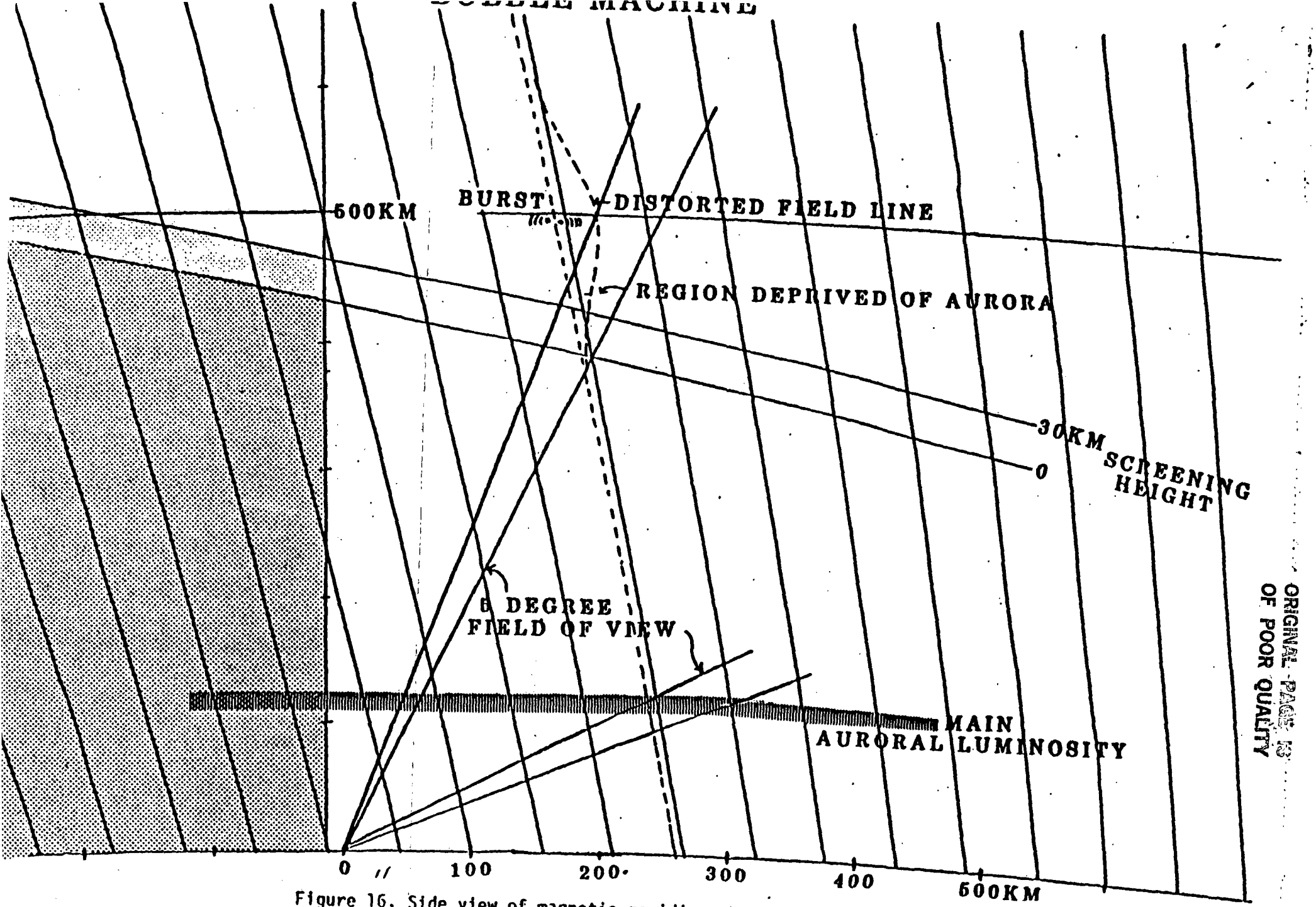

Figure 16. Side view of magnetic meridian showing the location of the Bubble Machine I burst point, the magnetic field lines, the fields of view of the two 4278A photometers from Ester Dome, Alaska, and the aurora.

Both the upper and lower photometer traces indicate an initial intensity reduction followed by an increase over the background level. If the injection initiated a magnetosonic wave train of a period of 5 sec., the first arrival at any point would be a compression of the magnetic field. An increase in the magnetic field would have the effect of raising the mirror height of the energetic electrons and vice versa, a following rarefaction of the field would lower the mirror height. This would also modulate the number of electrons precipitating and the volume emission rate.

Using the theory of Lutomirski (1978) we have calculated that the wave Bubble Machine I produced should have an amplitude near the burst of 40 nT. This is the order of magnitude registered by the electric field detector during the Bubble Machine II experiment of the following year. Assuming a 50 nT wave amplitude, the mirror height could be raised or lowered by 2.4 km, or an overall change of 4.8 km at the E layer.

Thus if modulation of the 4278A light is due to a magnetosonic wave, a larger amplitude wave than was measured in situ is suggested. Since the electric and magnetic field detectors were below the level of the burst plane and about 824 m from the field line intersection, it may be that the geometry reduced the amplitude of the ΔB at the mother payload.

Another possibility is that the electric field component of the 5 second period wavetrain has a small component parallel to B which might be effective in modulating the precipitating electrons.

B. In Situ Wave Observations on Bubble Machine II

We have already noted that the quasi-dc electric field signal implies that a modest amplitude Alfvén wave was produced in the expansion. As discussed below, the amplitude is not inconsistent with estimates based on the ground wave measurements.

The higher frequency waves shown in Figs. 10-12 show a good correlation with the optical data. For example, the signals below 100 Hz appear in two sets--one lasting about one second and the other abut 8 seconds--with about a two second gap between the emissions. Referring to Fig. 8, we can understand the emissions sequences as follows. The burst waves are associated with the explosion and leading edge of the ion ring. The low frequency waves ($\leq$ 120 Hz) probably lie on the density gradient. The gap in signal is totally consistent with the black hole since it should be absent of any barium related emissions. When the ion ring convects back across the payload some 2.5 seconds later, we again see the low frequency waves, this time clearly associated with the decreasing density gradient. The ratio of the durations of the two low frequency wave events are also consistent with an expansion/convection model associated with the ion ring.

As discussed in the next section, the burst waves may play a role in the black hole formation process. Here we investigate the lower frequency wave emission mechanism ($f \leq 120$ Hz). The barium plasma feels a radially outward force of the form

$$\underline{F} = m\nu_{in}\underline{u}_n$$

where $\underline{u}_n$ is the neutral expansion velocity and ν_{in} is the ion neutral collision frequency. This force is equivalent to a gravitational acceleration given by $\underline{g}' = \nu_{in}\,\underline{u}_n$ which is subject to the Rayleigh-Taylor (R-T) instability in regions of inward plasma density gradient ($\underline{g}'$ must be anti-parallel to $\underline{\nabla n}$).

The growth rate for the collisionless R-T process is

$$\gamma = (g'/L)^{1/2} \qquad (1)$$

while for the collisional R-T process it is

$$\gamma = g'/\nu_{in}L \qquad (2)$$

where L is the gradient scale length. The bounding ν_{in} relationship between the collisionless versus the collisional R-T process (Ott, 1978) is $\nu_{in}^* = 4u/L = 160$ Hz which, according to Fig. 5 is greater than ν_{in} at 100 ms. A transition thus occurs from a collisional process at early time to a collisionless process later. At t=1 sec, the optical data indicate L = 100 m while at .1 seconds it should be considerably smaller. If we let L=40 m and $u_n = 4000$ m/s and take $\nu_{in} = 75$ sec^{-1} (from fig. 5), we find $\gamma \gtrsim 80$ Hz which implies an e folding time of about 12 ms. Since the neutral gas is observed to be structured, there will certainly be initial finite perturbations to feed upon this energy source. The waves associated with this process should peak at kL = 1 which implies $\lambda = 300$ m. If we interpret the frequencies in Fig. 11 (spectrum 2) as Doppler shifted zero frequency turbulence (R-T waves have very low phase velocity), the break in the spectrum to a power law occurs at about 50 Hz which corresponds to wavelengths greater than about 100 m if the waves are being carried out at the expansion speed. Fluctuations are detected to about 1200 Hz which is roughly 3 m (under this same zero frequency hypothesis).

The wave spectrum number 4 is also quite interesting. First, the waves are located on the negative density gradient which corresponds to the unstable "leading edge" in the expansion phase. Second, this edge is further unstable to the $\underline{E} \times \underline{B}$ instability ($\underline{E} \times \underline{B}$ parallel to ∇n) as the structure convects back toward the northwest. At 1.06 km/s velocity, the very steep decrease in signal at 120 Hz corresponds to about 8 m wavelength. This is the gyro radius of a 1400° K barium ion in a .5 Gauss magnetic field.

The cutoff is so sharp that some characteristic frequency or scale must be involved. The ion gyro frequencies are all well below 120 Hz and the lower hybrid frequencies are all well above. It thus seems likely

that the 8 m barium gyro radius (r_i) is the important parameter. Furthermore, it is well known (Coppi, 1965) that finite ion gyro radius (FLR) effects stabilize the generalized Rayleigh-Taylor instability. A case can thus be made that the observed plasma structuring is due to a flute-mode Rayleigh-Taylor process initiated by the neutral gas expansion and perhaps sustained by the $\underline{E} \times \underline{B}$ instability after the expansion ceases.

Pursuing this line of argument further we may have tested a recent theoretical prediction by Sperling and Krall (1981) who investigated the "prompt striations" observed in a shaped charged experiment by Simons et al., (1980). They showed that the FLR stabilization only occurs if the ratio of background plasma density to the barium plasma density is above a certain threshold value. They argued then that in a low density background, short wavelength waves ($\lambda \sim r_i$) should occur early in the expansion process, creating the observed prompt striations. Our data is in excellent agreement with this proposal. For example, in the initial phase (spectrum 2) waves are present with a power law form between 3 m and a few hundred meters. Note that the gyro-radius associated with the <u>beam</u> velocity rather than the thermal velocity, is about 40 m. On the other hand when the expanding ring convects back to the payload we find no such power law and in fact an extremely sharp cut-off near r_i (the thermal value).

From Figures 1a-c of Sperling and Krall (1981) for the returning plasma, which has their parameter $\bar{\rho}/\rho_i \sim 0.1$, we can conclude quantitatively the short wavelength waves should be totally stabilized as observed. For the early phase it is more difficult to determine $\bar{\rho}/\rho_i$, the ratio of ambient mass density to beam mass density, but it certainly can only be a lower value which is consistent with the theory and the observed existence of short wavelength waves.

C. Black Hole Formation

The burst waves seem to be a mixture of electromagnetic and electrostatic waves with frequencies up to and in excess of the lower hybrid frequency. These may play a role in the black hole formation if the waves provide an anomalous coupling between the barium ions and the neutral gas. This can be seen as follows. The ion equation of motion is

$$nM_i d\underline{V}_i/dt = ne\underline{E} + ne(\underline{V}_i \times \underline{B}) + nM_i \nu_{in} \underline{u}_n$$

If $\nu_{in} > \Omega i$, the ions will follow the neutral gas and be swept out of the region near the explosion point. Now, classical collisions fall below Ωi within a few hundred ms. However, waves may destroy any organized gyro motion and allow efficient coupling to the neutrals. The waves themselves may be driven unstable by the modified two stream instability caused by the $\underline{E} \times \underline{B}$ streaming of electrons subject to the electric field pulse from the explosion. The threshold for this process would be about 40 mV/m for the conditions of the experiment.

The polarization E field due to the large gyroradius of the Ba+ ion with respect to the electrons and the coupling of this field to the conducting ionosphere below must be considered. The polarization field in the first approximation is radially inwards. It would propagate along the magnetic field at the Alfvén velocity. The Alfvén is estimated to be about 2000 km/sec at a nighttime electron density of 10^4 electrons/cc. Thus the polarization field could be shorted out in the ionosphere with a time delay of the order of 200 m sec. The field should have caused an upwards current near the burst point field line and downwards cylindrical current near the outer edge of the barium gas.

The current should primarily be carried by the electrons, but the net

effect would also be to accelerate Ba+ away from the plane of the explosion in a cylinder expanding in radius with time. The TV observations cannot confirm definitely the parallel to B motion due to the overwhelming brightness of the Ba neutral gas in the line of sight to the field line.

In Bubble Machine II the Cornell AC E field dipole measured some O+ lower hybrid resonance electrostatic waves up to about 500 m sec subsequently followed by a few seconds of waves at harmonics of the O+ gyrofrequency. The upper frequency limit of the AC detector was 15 kHz, so it was not possible to observe the occurrence of upper hybrid waves. The suggestion is made that small scale turbulence can be effective in allowing plasma transport across magnetic field lines.

The total effects of the momentum coupling of the neutral Ba gas and the explosive gas products to the Ba+ ions, the polarization field and coupling to the ionosphere with a time delay, may allow the ions to move outward freely to the 2.5 km radius required, or electrostatic turbulence may allow the ion motion. Self-consistent calculations on a big computer are required to answer the questions of the cause of black hole.

D. Discussion of E-Field Pulsations

It is tempting to identify the second wavelet as an echo of the original burst wavelet which has travelled along the field line to the opposite hemisphere and back. Periodic emissions in the Pc1 (0.3-3Hz) band are common at College, Alaska and exhibit repition times from two to five minutes. These are Alfvén waves which travel through the plasma in the ion cyclotron mode with a group velocity which depends upon the ion density of the magnetospheric plasma. The 140 second delay and the 5.5 second period observed in the telluric record are compatible with wave

patterns commonly observed on the L=5.5 shell at College. However, since no magnetic signature was observed, either at the rocket or at the ground, we cannot be certain that the detected pulses were electromagnetic. It is possible they represent electrostatic responses of the F-region wave guide to the burst.

It is, of course, possible that the wavelets are naturally occuring fluctuations detected by the telluric system. Since the recording system could only store 190 seconds of data we cannot check the data to see if similar pulses occurred 136 seconds before or 278 seconds afterwards. The wavelets at 2 and 140 seconds are the largest variations in the recording during the recording interval. The fact that they occur after the burst and that they are compatible with the common period and propagation ranges of waves observed at College give support to the interpretation that they were produced by the burst. Further, the observation of an oscillation of essentially the same five second period in the 4278A auroral emission following Bubble Machine I strengthens the case that these wavelets are burst-induced.

The burst occurred at an altitude of 460 km. One minute after the burst an ionogram was taken which showed spread-F features with foF of 4.2 MHz at 350 km with foF_E of 3.5 MHz at 110 km and no D layer. If we assume simple Alfvén wave propagation between the burst point and the E layer the ionogram allows us to estimate an Alfvén velocity $V_A \simeq 230$ km/sec and hence a propagation time of about 1.4 seconds from the burst point to the E region. This is less than the observed two second delay between the burst and the first wavelet in Figure 9. However it is of the same order as the time delay observed between the burst and E region response observed on Bubble Machine I.

Another effect to be considered is the size of the ion depleted region and the velocity of the slowest Ba gas. The black hole radius is about 2.5 km and the lowest gas velocity about 1 km/second. Thus it is plausible that the kinetic energy of the Ba gas is effective in compressing the magnetic field controlled plasma for about 2.5 seconds. The relaxation of the plasma and overshoot is consistent with a 5 second period oscillation continuing for several cycles before being damped out. However, the theory of Lutomirski (1968) would indicate that the slow moving plasma would be very inefficient in radiating hydromagnetic waves.

IV. Summary and Conclusions

The radial shaped charge experiments discussed in this paper made waves and created some other curious effects. Due to circumstances and limitations in the range of equipment fielded for each experiment effects were not observed on all three experiments. The formation of the black hole was best observed on King Crab because of the absence of any convection electric field to distort the ion configuration. However, stimulated auroral emissions and waves were masked by natural background noise at the burst time. The long period (5 second) modulation of 4278Å auroral emissions was only observed following Bubble Machine I, because no photometers were deployed during Bubble Machine II. Conversely the E field wave of period 5.5 seconds in telluric currents was only observed following Bubble Machine II, because no recordings were attempted during the other two experiments.

Examination of possible physical mechanisms for the creation of the ion-depleted black hole of radius about 2.5 km has not produced a viable explanation. Momentum transfer from the neutral gas to the ions can probably

move the ions out to a radius of about 500 m. Some other process allowed the ions to walk out another 2 km as if there were no magnetic field. There is insufficient energy in the gas to create a magnetic bubble that large, and the magnetic signatures is at most 50 nT in situ.

A possibility yet to be tested in a computer simulation is that the electron Hall drift was sufficient to set up a modified two stream instability producing small-scale turbulence. The high frequency waves might allow the plasma to walk out the additional two kms.

The injection of the plasma radially apparently excited an eigen-frequency wave of period about 5 sec. In Bubble Machine I this was evidenced by modulation of the electron precipitatin causing 4278A auroral emissions. Based on a one second delay between the modulation near the burst, and in the E region at the foot of the field line, the propagation velocity was about 380 km/sec, within the Alfvén propagation range. The magnetic pertubation does not seem large enough to raise or lower the mirror height sufficiently to account for the 50% modulation in luminosity. We suggest that a small E field component of the wave, parallel to Be, could more efficiently modulate the flow of electrons.

The second manifestation of the 5 second period wave was in telluric field recordings during Bubble Machine II. The two cycle wavelet commenced 2 seconds after the burst, and was followed 138 seconds later by what we conclude is probably a wave reflected from the southern hemisphere ionosphere with about 1/2 amplitude. The ionospheric density deduced from an ionogram taken one minute after detonation would predict a burst to E layer propagation of 230 km/sec, which would account for a time delay of 1.4 seconds instead of the two seconds observed. The frequency, interhemisphere bounce time

and F to E layer propagation velocity are well within observed values of natural waves at L = 5.5 for ion-cyclotron mode waves.

Acknowledgements

We wish to thank the personnel of NASA Wallops Flight Center and in paticular Jay Brown the payload manager for payload fabrication and launch support. We also thank the personnel of NASA Ames Flight Center for the use of the NASA Lear Jet for TV observations. The help of the personnel of Poker Flat Rocket Range is gratefully acknowledged. Mr. DuWayne Bostow was instrumental in managing the high explosive shaped charge payload components and in fabricating the barium metal liners. Mr. Gale Weeding of Falcon Research and Denver Research Institutes made the high explosive shaped charges. We thank Mr. Hal Hannigan of Explosive Technology for his help in providing the accurate simultaneous detonation train. We also appreciate the cooperation of the U.S. Air Force Military Air Transport for transportation of barium and high explosives. We acknowledge the important contribution of Gary Meltvedt in the TV logistics and observations. We also wish to express our appreciation to Los Alamos National Laboratory for machining the barium liners in the King Crab device.

The work by Cornell University was supported by NASA Grant NSG 6020, and the work by the University of California at San Diego was supported by NASA Grant NAG 5-610. The work of the Geophysical Institute was supported by NASA Grant NAG 6-1 and in part by the Defense Nuclear Agency.

REFERENCES

Alfvén, H., On the Origin of the Solar System, Oxford University Press, Oxford, 1954.

Alfvén, H., and G. Arrhenius, Structure and Evolution History of the Solar System, D. Reidel Publ. Co., Amsterdam, 1975.

Cook, M. A., The Science of High Explosives, Robert E. Krieger Publ. Co. Inc., Huntington, N.Y. p. 306, 1971.

Coppi, B., Instibilities induced by particle collisions in confined plasmas, in Nonequilibrium Thermodynamics, Variational Techniques and Stability, ed. R. J. Donnely, p. 259, Univ. of Chicago Press, Chicago, IL, 1965.

Cresswell, G. R., Fast auroral waves, Planet Space Sci. 16, p. 1453-1464, 1968.

Deehr, C. S. and Romick, G. J., Pulsating aurora induced by upper atmosphere barium releases, Nature, 267, 135-136, 1977.

Deehr, C. S., E. M. Wescott, H. C. Stenbaek-Nielsen, G. J. Romick, T. J. Hallinan and H. Föppl, A critical velocity interaction between fast barium and strontium atoms and the terrestrial ionospheric plasma, Geophys. Res. Lett., 9(3), pp. 195-198, 1982.

Gorney, D. J., A. Clarke, D. Croley, J. Fennell, J. Luhmann, and P. Mizera, The distribution of ion beams and conics below 8000 km, J. Geophys Res., 86, 1981

Haerendel, G., Critical velocity experiments in Space, Proceedings of Workshop on Alfvén's Critical Velocity Effect, Max Planck Institut fur extraterrestrische Physik, ISSN 0340-8922, P. 216, 1982.

Holmgren, G., R. Bostrom, M. C. Kelley, P. M. Kintner, R. Lundin, U. V. Fahleson, E. A. Bering and W. R. Sheldon, Artificial stimulation of auroral electron acceleration by intense field aligned currents, Geophys. Res. Lett., 6, 789, 1979.

Holmgren, G., R. Bostrum, M. C. Kelley, P. M. Kintner, R. Lundin, U. V. Fahleson, E. A. Bering and W. R. Sheldon, Trigger, an active release experiment that stimulates auroral particle percipation and wave emissions, J. Geophys. Res., 4469, 1982.

Kelley, M. C., U. V. Fahleson, G. Holmgren, R. Bostrom, P. M. Kintner, and E. Kudeki, Generation and propagation of an electromagnetic pulse in the Trigger experiment and its possible role in electron acceleration. J. Geophys. Res., 85, 5055-5060, 1980.

Lundin, R., G. Holmgren, Rocket observations of stimulated electron acceleration associated with the Trigger experiment, J. Geophys. Res., 85, 5061, 1980.

Lutomorski, R. F., A model for the generation of magneto-hydromagnetic waves by high altitude nuclear bursts, J. Geophys. Res., 73, (15),4943-4957, 1968.

Michel, K. W., Verhalten der Ba-Ionenstrahlen aus Hohlladungen beirn Nike-Tomahawk Experiment, Max-Planck-Institut für Physik und Astrophysik, MPI-PAE Extraterr. 19, 1969.

Michel, K. W., Fluorescent ion jets for studying the ionosphere and magnetosphere, Acta Astronautica I(1) p. 37-69, 1974.

Ott, E., Theory of Rayleigh-Taylor bubbles in the equatorial ionosphere, J. Geophys. Res., 83, 2066, 1978.

Simons, D. J., M. B. Pongratz, and S. P. Gary, Prompt striations in ionospheric barium clouds due to a velocity space instability, J. Geophys. Res., 85, 671, 1980.

Sperling, J. L. and N. A. Krall, Stabilization of electrostatic, purely growing, finite ion gyroradius, flute instabilities in the ionosphere, J. Geophys. Res., 86, 7513, 1981.

Wescott, E. M., H. C. Stenbaek-Nielsen, T. J. Hallinan, C. S. Deehr, G. J. Romick, J. V. Olson, J. G. Roederer and R. Sydora, A high altitude barium radial injection experiment, Geophys. Res. Lett., 7(12), pp. 1037-1040, 1980.

Yau, A. W., B. A. Whalen, A. G. McNamara, P. J. Kellogg, W. Bernstein, Particles and wave observations of law-altitude ionospheric ion acceleration events, J. Geophys. Res., 88, 1983.

FIGURE CAPTIONS

Figure 1. Cross section schematic drawing of radial high explosive shaped charge used in Bubble Machine I and II. Detonation is at the center causing the liner to collapse and Ba gas to jet out horizontally with radial symmetry.

Figure 2. Differential Ba atom numbers vs radial velocity distribution, Bubble Machine II, derived from TV signal level scans. Fifteen per cent vaporiztion of liner was assumed to assign number scale value.

Figure 3. Side view of Bubble Machine II from geophysical Institute TV on NASA Ames Learjet, 21.5 sec. after detonation. The plane of the low velocity Ba gas doughnut is 17° with respect to the viewer and the distance is 1950 km. The two stars are π Andromeda and B.S. 157.

Figure 4. TV view of the stellate ion structure produced in the March 16, 1980 King Crab experiment 205 seconds after detonation. The inner hub region depleted of ionization is called a black hole. An almost complete absence of an ionospheric E field allowed the structure to be seen for about 20 minutes.

Figure 5. Plots of the differential kinetic energy vs velocity, Bubble Machine II experiment and the collision frequency between a barium ion and the streaming neutral barium gas at 100 msec after the burst. Note that although the highest energy is centered near 4 km/sec., collisions are too infrequent to couple energy from the neutral gas to the ions and magnetic field. Energy can be transferred near the low velocity peak near 1-2 km/sec.

Figure 6. Comparison of 5° field of view photometers with 4278Å interference filters looking near the Bubble Machine I burst region (upper trace) and in the 110 km region near the foot of the burst point field line. Note the one second phase shift between the upper and lower traces. A damped oscillation in the 4278Å emission with about a 5 second periodicity commences with a decrease.

Figure 7. Geophysical Institute TV picture of Bubble Machine II at +5 seconds from Fort Yukon, Alaska. Note the regions of blob-like irregularities.

Figure 8. Plan view of part of the ion ring surrounding the black hole of Bubble Machine II at one second intervals. The position is due to the forces acting to push the ions outwards to about 2.5 km and the EXB drift to the northwest. As a result the ions would sweep across the instrumented payload for about 300 ms then return starting about 2.5 seconds after burst.

Figure 9. Recording of the voltage across a 1.6 km grounded dipole oriented close to magnetic north south at Poker Flat, Alaska, during the Bubble Machine II event. The two cycle pulsation commencing two sec. after burst appears to be a result of the explosive Ba perturbation The two cycle wave commencing at 140 sec. is consistent with Alfvén wave propagation to the southern conjugate ionosphere and return.

Figure 10. A VLF sonogram showing electric field fluctuations intensity as a function of time and frequency.

Figure 11. A low frequency sonogram showing the low frequency waves and representative power spectrum.

Figure 12. Integrated electric field and density fluctuation signal strengths versus time.

Figure 13. The bottom panel shows the flux of ions at the energy per charge shown in the bottom panel for about one second after the chemical ignition. All of these ions are at nearly 0 degree pitch angle.

Figure 14. The flux of electrons at 240 ev at the given pitch angle in the top panel.

Figure 15. Volume emission rate of 4278Å vs altitude, Bubble Machine I. Solid line is the normal contribution of the precipitating electrons. The dashed curve is the fluorescence scattering in the sunlit position.

Figure 16. Side view of magnetic meridian showing the location of the Bubble Machine I burst point, the magnetic field lines, the fields of view of the two 4278Å photometers from Ester Dome, Alaska, and the aurora.